

CHAPTER 1

**JET QUENCHING AND RADIATIVE ENERGY LOSS
IN DENSE NUCLEAR MATTER**

Miklos Gyulassy¹, Ivan Vitev², Xin-Nian Wang³ and Ben-Wei Zhang⁴

¹*Department of Physics, Columbia University, 538 W. 120th Street,
New York, NY 10027*

²*Department of Physics and Astronomy, Iowa State University,
Ames, IA 50010*

³*Nuclear Science Division, MS 70R0319,
Lawrence Berkeley National Laboratory, Berkeley, CA 94720*

⁴*Institute of Particle Physics, Huazhong Normal University,
Wuhan 430079, China*

We review recent finite opacity approaches (GLV, WW, WOGZ) to the computation of the induced gluon radiative energy loss and their application to the tomographic studies of the density evolution in ultra-relativistic nuclear collisions.

1. Introduction

Since June 2000 measurements of $Au + Au$ reactions at the Relativistic Heavy Ion Collider (RHIC) at the Brookhaven National Laboratory (BNL) at $\sqrt{s} = 56, 130, 200$ AGeV (GeV per nucleon pair) have revealed a variety of novel multiparticle phenomena not observed previously in e^+e^- , ep , pp collisions at any energy nor in nuclear collisions at lower (SPS/CERN and AGS/BNL) energies ($\sqrt{s} = 17, 5$ AGeV). While the bulk global observables such as the rapidity dependence of hadron multiplicities and transverse energy scale geometrically from elementary $p + p$ collisions, the most striking new phenomena were discovered in rare high transverse momentum observables^{1–9}. The preliminary RHIC data are discussed extensively in the Quark Matter 2001 and 2002 proceedings¹⁰.

At RHIC collider energies the hard pQCD rate of rare high p_T parton scattering becomes sufficiently large that jets can be used to probe the dense quark-gluon plasma formed in nuclear collisions. In 1982 Bjorken proposed

that elastic final state energy loss of partons may “extinguish” jets in high energy $p + p$ collisions¹¹. However, the elastic energy loss of partons in a QCD plasma of temperature $T \sim 300$ MeV turned out to be too small ($dE_{el}/dx < 500$ MeV/fm)^{12,13} for jet extinction. The data on $p + p$ jets up to Tevatron energies show no sign of deviations from unquenched factorized pQCD. Di-jet acoplanarity was proposed as another possible manifestation of elastic final state interactions^{14,15,16}. Prior to current RHIC data on nuclear collisions at 200 AGeV, the data showed no hint of this effect.

In some early studies^{17,18,19} it was suggested that induced radiative energy loss in nuclear collisions could be much larger than the elastic energy loss and jet quenching should become observable at least in collisions of heavy nuclei. With the development of the Monte Carlo HIJING event generator^{20,21,22}, predictions for the magnitude of the suppression pattern high p_T hadrons were made in a first study²³ as shown in Fig. 1. The middle panel shows that up to an order of magnitude suppression of charged hadrons was expected in the moderate $p_T \sim 5$ GeV range. The input assumption was that the gluon energy loss in the plasma was $dE/dx = 2$ GeV/fm due to induced gluon radiative energy loss. The HIJING model is a two component model with semi-hard and hard pQCD jet above $p_T > p_0 = 2$ GeV computed via the PYTHIA code and the “soft” beam jet fragments computed via a hybrid LUND and Dual Parton model algorithm. See the original article²⁰ for a detailed discussion and references.

A selection of recent data from RHIC that confirm strong nuclear attenuation of moderate high transverse momentum charged hadron and π^0 production are shown in Fig. 2 through Fig. 5. In order to appreciate just how remarkable and different this experimental discovery is relative to previous lower energy data from the SPS, the quenching pattern of π^0 measured at RHIC is compared in Fig. 4 to the strong *enhancement* of high p_T π^0 measured in $Pb + Pb$ at 17 AGeV at the SPS²⁴.

The enhancement of high p_T hadrons at SPS is an amplified version of the well known Cronin effect first observed in $p + A$ collisions. As we elaborate in later sections, it is due to multiple *initial* state interactions and completely masks any possible energy loss effects at the SPS. In contrast, at RHIC the high energy loss overwhelms the Cronin enhancement in our present interpretation of the data.

As discussed for example in Refs.^{25,26}, it is useful to decompose the nuclear geometry dependence of invariant hadron distributions produced in $A + B \rightarrow h + X$ at impact parameter b into a phenomenological “soft”

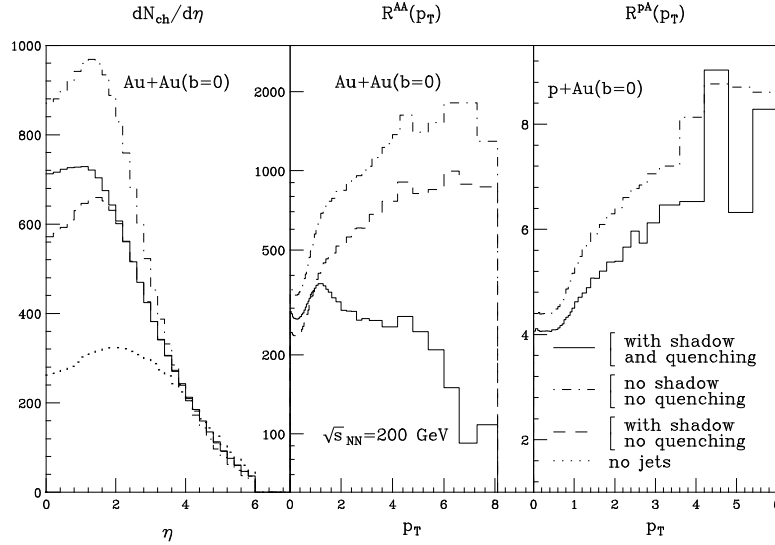
JET QUENCHING AND RADIATIVE ENERGY LOSS IN DENSE NUCLEAR MATTER³

Fig. 1. HIJING predictions²³ of the inclusive charged hadron spectra in central $Au+Au$ and $p+Au$ collisions at $\sqrt{s} = 200$ AGeV. The competing effects of minijet production (dash-dotted), gluon shadowing (dashed) (assuming that gluon shadowing is identical to that of quarks), and jet quenching (solid) with $dE/dx = 2$ GeV/fm are shown. $R^{AB}(p_T)$ is the ratio of the inclusive p_T spectrum of charged hadrons in $A+B$ collisions to that of $p+p$. In contrast to $Au+Au$, no significant quenching is expected in $p+Au$ (or $d+Au$) since only $\sim 20\%$ initial state shadowing and Cronin effects modify the pQCD spectrum at high p_T .

and perturbative QCD calculable “hard” components as

$$E \frac{dN_{AB}(b)}{d^3p} = \frac{N_{part}(b)}{2} \frac{dN_{soft}(b)}{dy d^2\mathbf{p}_T} + N_{coll}(b) \frac{1}{\sigma_{in}^{pp}} \frac{d\sigma_{hard}(b)}{dy d^2\mathbf{p}_T}, \quad (1)$$

where $N_{part}(b)$ is the number of nucleon participants and $N_{coll}(b) = \sigma_{in}^{pp} T_{AB}(b)$ is the number of binary NN collisions at impact parameter b . The nuclear geometry of hard collisions is expressed in terms of the Glauber profile density per unity area $T_{AB}(b) = \int d^2\mathbf{r} T_A(\mathbf{r}) T_B(\mathbf{r} - \mathbf{b})$ where $T_A(r) = \int dz \rho_A(\mathbf{r}, z)$ (see Fig. 6). The hard part scales with the number of binary collisions $\propto A^{4/3}$ because the probability of high p_T processes is small and built up from all possible independent parton scattering processes. The soft part scales with only $N_{part} \propto A$ because the probability of low transverse momenta processes is bounded by unitarity. This is sometimes referred to as Glauber shadowing or saturation depending on the calculational frame. The “soft” part is actually the overwhelming

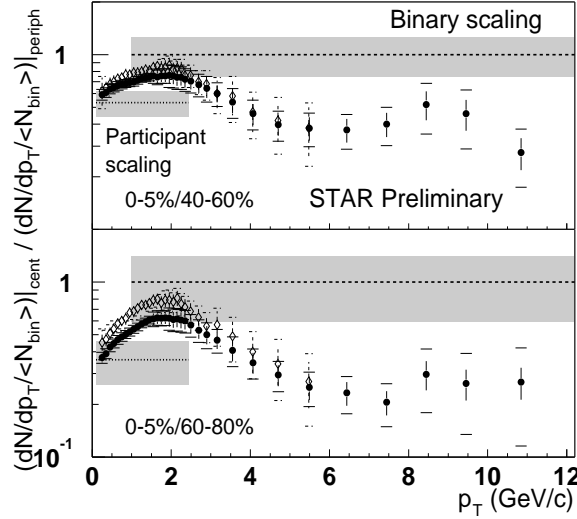


Fig. 2. Preliminary STAR⁵ data on charged hadron quenching between central and peripheral $Au + Au$ collisions at $\sqrt{s} = 200$ AGeV is shown for peripheral event classes. The data are scaled by the Glauber binary collision scaling factor for each centrality class. Upper gray band is the expected result from pQCD scaling from $p + p$. Lower gray bands correspond to scaling with the nucleon participant number instead. Beyond 4 GeV, charged hadrons are suppressed by 0.2-0.4 (factor 2.5 to 5) relative to naive binary scaling.

bulk of the produced hadron distribution. It is expected to reflect the collective hydrodynamic properties of the produced plasma in $A + A$ collisions. Relativistic hydrodynamics predicts specific flow patterns, such as hadron mass dependent transverse elliptic flow^{31,32,33,34}, which may provide direct constraints on the QCD equation of state. Unfortunately, low transverse momentum processes are not directly computable via QCD and many competing phenomenological models can be adjusted to fit the data not only at RHIC but SPS and AGS as well.

The great advantage of RHIC over the previous AGS and SPS explorations of nuclear collisions is that the computable high p_T pQCD processes are sufficiently abundant, and that they can be used as effective “external probes” of the quark-gluon plasma that is produced. High p_T and heavy mass partons are produced first, at time $\delta\tau \sim 1/m_T$ fm/c, while the most of the partons of the plasma with temperature T form and equilibrate at later times $\sim 1/gT \sim 0.5$ fm/c. Hard jets propagate along approximate

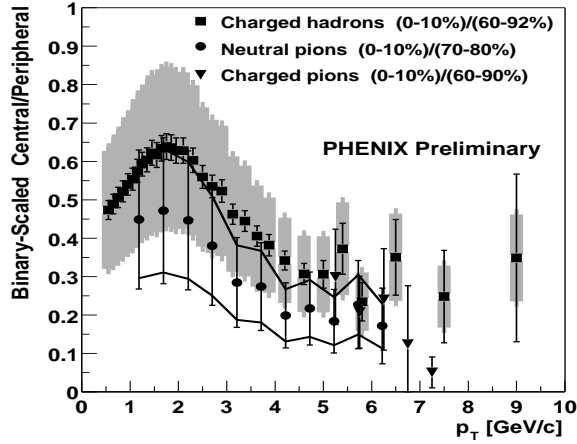
JET QUENCHING AND RADIATIVE ENERGY LOSS IN DENSE NUCLEAR MATTER⁵

Fig. 3. Preliminary PHENIX³ data on charged and π^0 hadron quenching between central and peripheral $Au + Au$ collisions at $\sqrt{s} = 200$ AGeV is shown. The pions are generally more quenched than the summed charged hadrons ($\pi + K + p$).

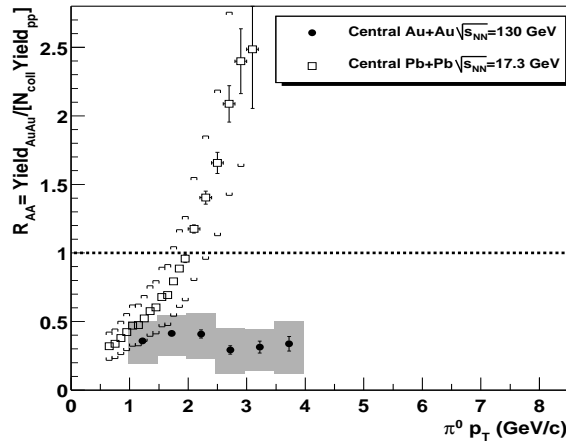


Fig. 4. The striking contrast between PHENIX¹ data on π^0 quenching in central $Au + Au$ collisions at $\sqrt{s} = 130$ AGeV compared to the (Cronin) enhancement found in $Pb+Pb$ at 17 AGeV from²⁴ demonstrates that jet quenching is a new nuclear phenomenon first seen at RHIC.

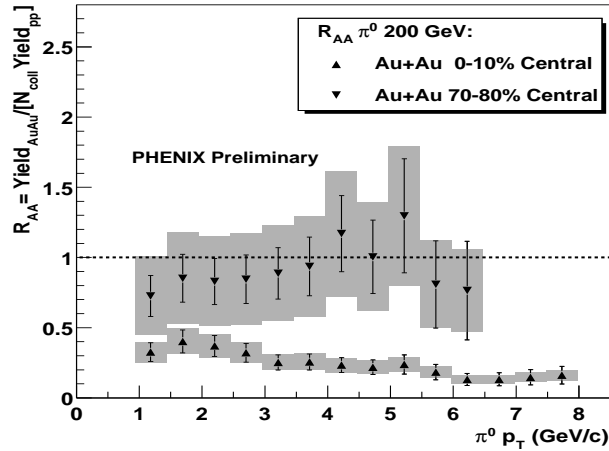


Fig. 5. Preliminary $\sqrt{s} = 200$ AGeV PHENIX³ data on π^0 quenching on central and peripheral $Au + Au$ collisions is compared relative to preliminary PHENIX data on $p + p$. Peripheral reactions are consistent with simple binary ($\sim A^{4/3}$) scaling from $p + p$ while in central collisions substantial quenching is observed.

straight eikonal lines through the plasma until $\tau \sim R \sim 5$ fm/ c . The energy loss and transverse momentum broadening suffered by the jet prior to hadronization provides the tomographic handle to probe the opacity of the evolving plasma. Since non-central collisions have a well known geometrical asymmetry, the azimuthal distribution of final high p_T hadrons provides even more information^{35,36}. This is illustrated in Fig. 7 by the normalized average thickness of nuclear matter as a function of the angle with respect to the reaction plane that a fast parton sees on its way out. The azimuthal distribution can be Fourier decomposed into

$$\frac{dN(b)}{dyd^2\mathbf{p}_T} = \frac{1}{\pi} \frac{dn(b)}{dydp_T^2} (1 + 2v_1(y, b, p_T) \cos(\phi - \phi_b) + v_2(y, b, p_T) \cos(2(\phi - \phi_b)) + \dots), \quad (2)$$

where ϕ_b is the azimuthal angle of the impact parameter b . In Fig. 8 the large elliptic flow component v_2 is seen to extend up to the highest p_T in non-central collisions at mid-rapidity. Another critical new experimental test for jettiness at moderate $p_T \sim 5$ GeV is provided by two particle correlation. The data from both STAR and PHENIX show clear evi-

JET QUENCHING AND RADIATIVE ENERGY LOSS IN DENSE NUCLEAR MATTER

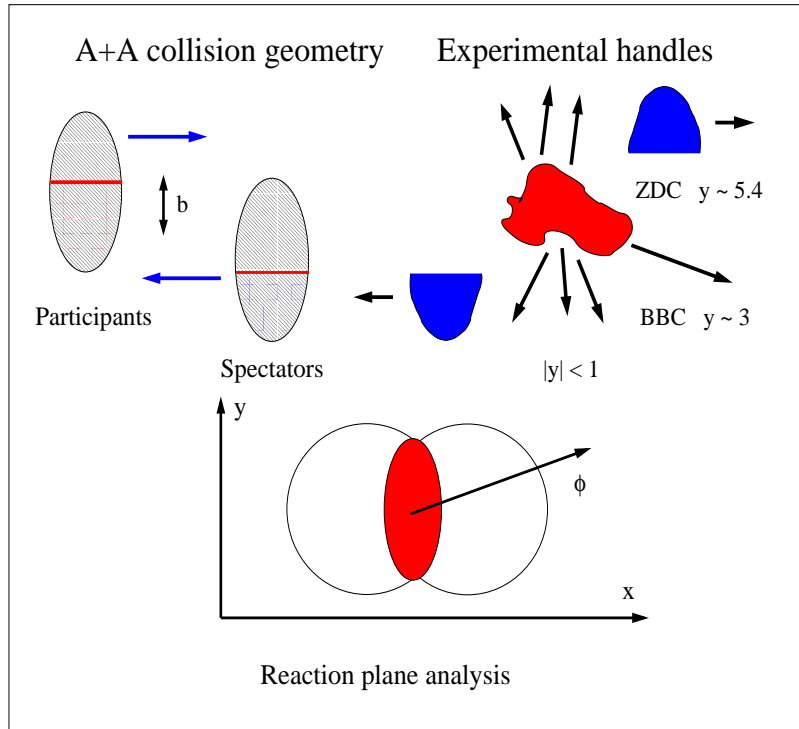


Fig. 6. Illustration of key aspects of the relation between the geometry of nuclear collisions and the participant $N_{part}(b) = 2 \int d^2r T_A(b-r)(1 - \exp(-\sigma^{pp}T_A(b))) \sim A^1 \leq 2A$ and collision $N_{coll}(b) = \sigma^{pp}T_{AA}(b) \sim A^{4/3}$ number at a fixed impact parameter. The observables $dN^{ch}/d\eta$, $dE_T/d\eta$, $v_2(p_T)$ (see Refs.^{27,28,29,30}) used to constrain the geometry experimentally are also illustrated.

dence for back-to-back correlations predicted by pQCD (and checked via the PYTHIA generator). However, there appears to be a difference between the correlation pattern of charged and neutral hadrons as seen in Figs. 9 and 10. The STAR data are in accord with predictions in Refs.^{17,18,37} that the two jet structure should be quenched by an order of magnitude relative to jet correlations in $p + p$ due to the high opacity of the plasma. Similar jet structure in high p_T neutral hadron correlations is also found in the preliminary PHENIX data⁴. Whether the suppression of away-side jet seen in STAR data also manifests in the PHENIX experiment has yet to be addressed.

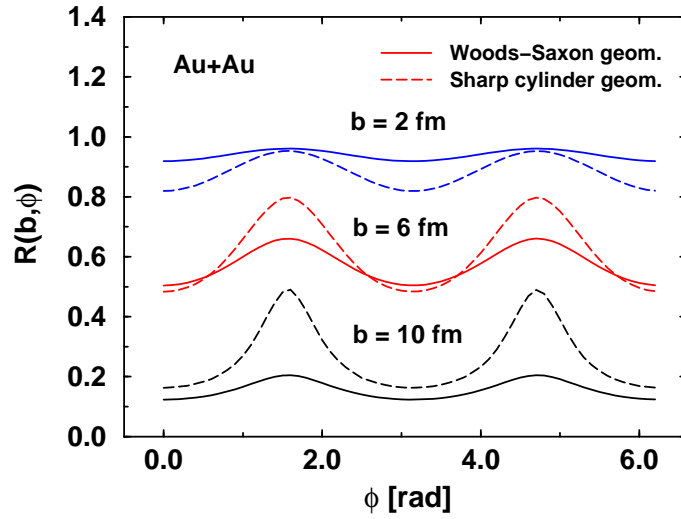


Fig. 7. The average normalized optical depth (R from Fig. 2 of Ref.³⁶) seen by a parton propagating through a plasma in azimuthal direction ϕ for different impact parameters and different density profiles.

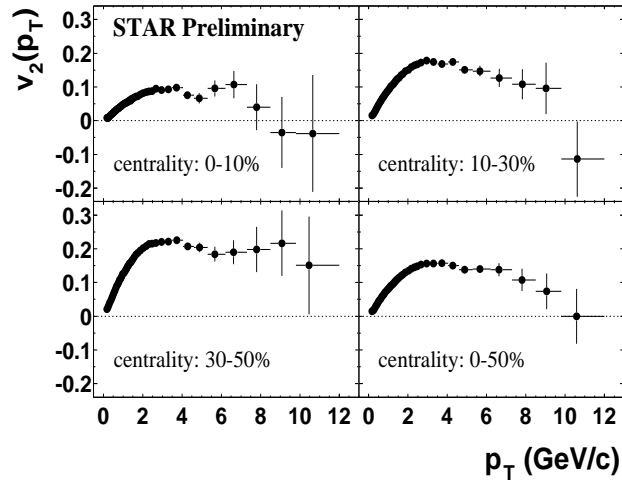


Fig. 8. Preliminary $\sqrt{s} = 200$ AGeV STAR⁵ on high p_T elliptic flow is shown. A value of $v_2 = 0.2$ corresponds to a 2-to-1 azimuthal asymmetry of hadrons.

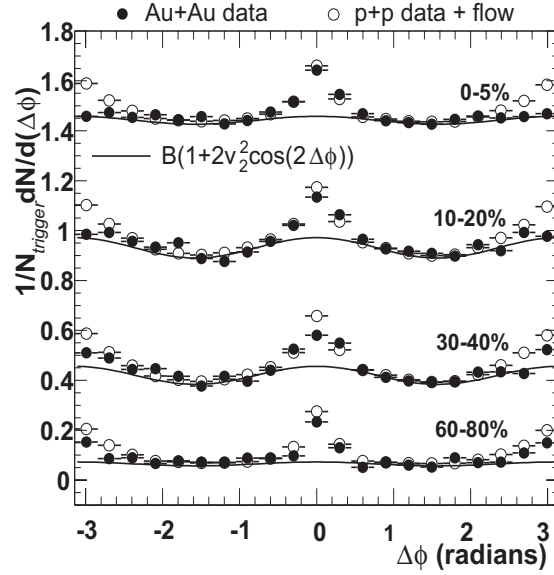
JET QUENCHING AND RADIATIVE ENERGY LOSS IN DENSE NUCLEAR MATTER⁹

Fig. 9. STAR data on high p_T azimuthal correlations of charged hadrons at 200 AGeV from Ref.⁶ showing clear evidence near side and away side correlations characteristic of two jet production in elementary $p + p$. However, in $Au + Au$ reactions the away side jet correlations are reduced in central collisions. The Back-to-Back jet correlations are attenuated by an order of magnitude in the most central collisions as expected if the plasma produced is opaque^{17,18,37}.

For our review, the most important point about both data sets is that narrow azimuthal near side and away side correlations do exist. This is a necessary (though not sufficient) conditions to enable us to interpret moderate p_T hadronic quenching patterns as due to jet energy loss.

In this review we focus on the rare hard pQCD tail of the hadron yields where all these interesting new nuclear phenomena have been discovered at RHIC. The central element of the theory that will be elaborated in the following sections is the predicted dependence of the induced QCD radiative energy loss on the jet energy, the plasma density, and the expansion properties of the plasma. We restrict the discussion to two complementary approaches, the GLV and WW/WOGZ formalisms, that are best suited in our opinion to applications to nuclear collision problems where the opacity is necessarily finite and the energy range of minijets accessible experimen-

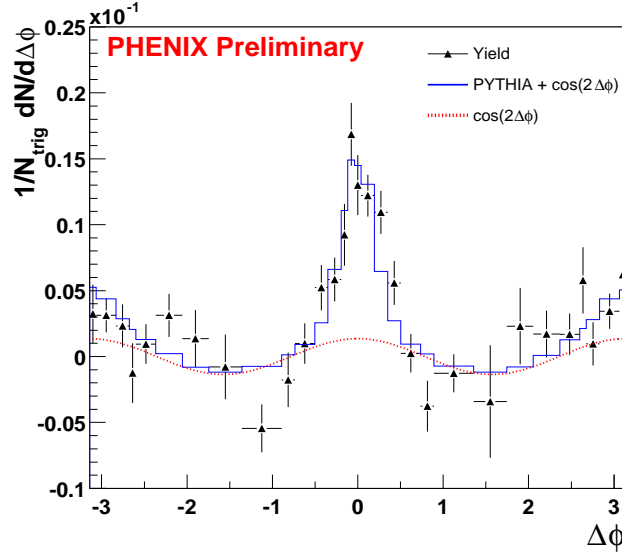


Fig. 10. Preliminary PHENIX data⁴ on high p_T azimuthal³⁶ correlations of *neutral* pions also show clear jet structure amid an elliptic flow component.

tally is typically 3 – 15 GeV.

In the absence of final state interactions we recall the well-known lowest order invariant pQCD differential cross section for inclusive $p + p \rightarrow h + X$ given by

$$E_h \frac{d\sigma_{hard}^{pp \rightarrow h}}{d^3p} = K \sum_{abcd} \int dx_a dx_b f_{a/p}(x_a, Q_a^2) f_{b/p}(x_b, Q_b^2) \times \frac{d\sigma}{dt}(ab \rightarrow cd) \frac{D_{h/c}(z_c, Q_c^2)}{\pi z_c}, \quad (3)$$

where $x_a = p_a/P_A$, $x_b = p_b/P_B$ are the initial momentum fractions carried by the interacting partons, $z_c = p_h/p_c$ is the momentum fraction carried by the final observable hadron, $f_{\alpha/p}(x_\alpha, Q_\alpha^2)$ are the parton distribution functions (PDFs), and $D_{h/c}(z_c, Q_c^2)$ is the fragmentation function (FFs) for the parton of flavor c into h .

The phenomenological K factor is introduced to mimic next-to-leading order (NLO) corrections. One finds that Eq.(3) tends to over-predict the curvature of the inclusive hadron spectra in the $p_T \leq 4$ GeV range. This can be partially corrected via the intrinsic k_T -smearing of partons associated with vacuum radiation and generalized parton distributions $\hat{f}_\alpha(x, k_T, Q^2)$.

JET QUENCHING AND RADIATIVE ENERGY LOSS IN DENSE NUCLEAR MATTER 11

For the corresponding modification of the kinematics in (3) in addition to the $\int d^2k_T^a \int d^2k_T^b (\dots)$ see Refs.^{38,39}. The generalized parton distributions are often approximated as

$$\tilde{f}_\alpha(x, k_T, Q^2) \approx f_\alpha(x, Q^2)g(k_T), \quad g(k_T) = \frac{e^{-k_T^2/\langle k_T^2 \rangle}}{\pi \langle k_T^2 \rangle}, \quad (4)$$

where the width $\langle k_T^2 \rangle$ of the Gaussian is related to initial state vacuum radiation. Discussion of some qualitative features of $\langle k_T^2 \rangle_{pp}$ is given in Refs.^{39,40}. For comparison to experimental data the reader is referred to Refs.^{39,41,42}. Fig. 11 shows that this parton model approach provides a good description of the high p_T data on hadron production in the range above a few GeV at all center of mass energies.

In order to calculate the effects of parton energy loss on the attenuation pattern of high p_T partons in nuclear collisions, we must modify the free space fragmentation functions^{39,43}. Energy loss of the parton prior to hadronization changes the kinematic variables of the effective fragmentation function. In the first approximation, this effect can be taken into account by replacing the vacuum fragmentation functions in Eq.(3) by effective quenched ones^{44,45}

$$z_c D'_{h/c}(z_c, Q_c^2) = z'_c D_{h/c}(z'_c, Q_{c'}^2) + N_g z_g D_{h/g}(z_g, Q_g^2);$$

$$z'_c = \frac{p_h}{p_c - \Delta E_c(p_c, \phi)}, \quad z_g = \frac{p_h}{\Delta E_c(p_c, \phi)/N_g}, \quad (5)$$

where z'_c, z_g are the rescaled momentum fractions. The first term is the fragmentation function is of the jet c after losing energy $\Delta E_c(p_c, \phi)$ due to *medium induced* gluon radiation. The second term is the feedback due to the fragmentation of the $N_g(p_c, \phi)$ radiated gluons. The modified fragmentation function satisfies the light-cone sum rule $\int dz_c z_c D'_{h/c}(z_c, Q_c^2) = 1$. Eq.(5) takes into account the dependence of the energy loss on the parent parton energy and the possibly azimuthally asymmetric region of high density nuclear matter.

In the above first approximation, only the average value of the energy loss is used. One can also include multigluon fluctuations^{46,47} of the energy loss via an energy loss distribution $P(\epsilon, E)$ where $\epsilon = \sum_i \omega_i/E$ is the fractional energy loss of a jet of energy E in the rest frame of the plasma. The mean energy loss in the first approximation is related to P via

$$\int_0^\infty d\epsilon P(\epsilon, E)\epsilon = \Delta E/E. \quad (6)$$

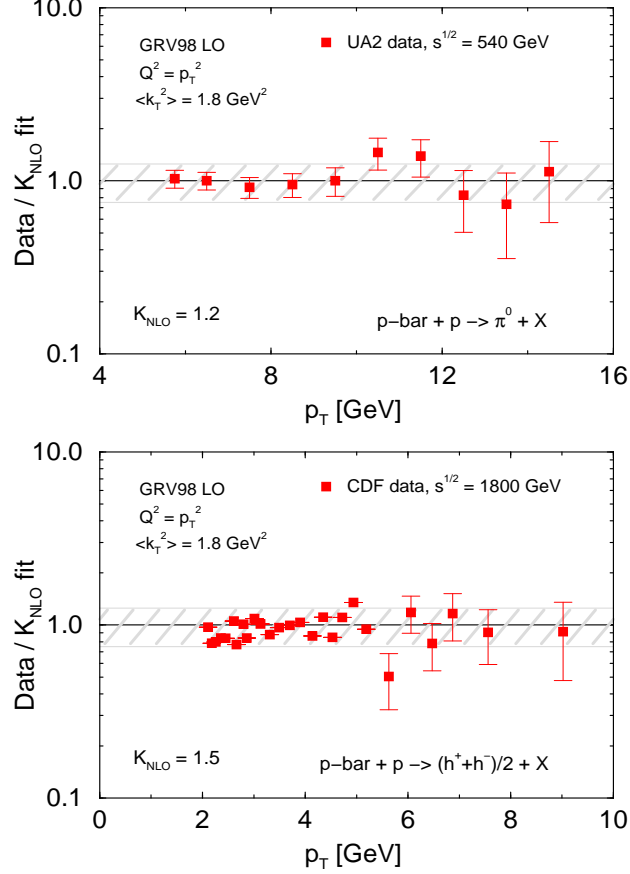


Fig. 11. Comparison of the pQCD model⁴² with intrinsic $\langle k_T^2 \rangle = 1.8 \text{ GeV}^2$ and GRV 98 PDFs to $\bar{p}+p$ data at $\sqrt{s} = 540, 1800 \text{ GeV}$. The normalization K factor simulating higher order corrections is fit at each energy. A $\pm 25\%$ error band is also included.

The invariant hadron distribution attenuated by fluctuating energy loss in $A + A$ collision is then given by

$$\begin{aligned}
 E_h \frac{dN_h^{AA}}{d^3p} &= T_{AA}(b) \sum_{abcd} \int dx_1 dx_2 \int d^2\mathbf{k}_a d^2\mathbf{k}_b g(\mathbf{k}_a) g(\mathbf{k}_b) \\
 &\times S_A(x_a, Q_a^2) S_B(x_b, Q_b^2) f_{a/A}(x_a, Q_a^2) f_{b/B}(x_b, Q_b^2) \\
 &\times \frac{d\sigma^{ab \rightarrow cd}}{dt} \int_0^1 d\epsilon P(\epsilon) \frac{z_c^*}{z_c} \frac{D_{h/c}(z_c^*, Q_c^2)}{\pi z_c}, \quad (7)
 \end{aligned}$$

where $z_c^* = z_c/(1 - \epsilon)$. Here, $T_{AA}(b)$ is the Glauber binary collision profile density at impact parameter b . It is found numerically⁴⁷, that fluctuations tend to reduce the magnitude of the attenuation by a factor about two at RHIC. It is important to include this effect when inverting the attenuation pattern in jet tomography to determine the initial plasma density. In $B + A$ reactions isospin effects can be accounted for a nucleus with Z protons and N neutrons by $f_{\alpha/A}(x_\alpha, Q_\alpha^2) = (Z/A) f_{\alpha/p}(x_\alpha, Q_\alpha^2) + (N/A) f_{\alpha/n}(x_\alpha, Q_\alpha^2)$. Nuclear modifications to the PDFs are estimated in our applications by using the shadowing function $S_A(x_\alpha, Q_\alpha^2)$ proposed by EKS'98⁴⁸.

2. GLV Theory of Radiative Energy Loss

In this section we turn to the theoretical problem of computing the energy loss of a fast parton penetrating a finite, expanding quark-gluon plasma. High p_T many body pQCD is a new frontier of research at RHIC and eventually LHC. The needed new theoretical development is the non-Abelian analogue of the radiative energy loss theory familiar from classical E&M. An important practical problem in QCD is that there exists no external beam of isolated colored quarks or gluons, and that the jets are always produced in hard processes just before the plasma is created. In addition, the nuclear medium has a small dimension compared to the jet fragmentation coherence length. Therefore, the basic formation time physics of Landau-Pomeranchuk-Migdal^{49,50,51} (LPM) is expected to lead to strong destructive interference effects that have to be carefully taken into account.

In this section we review one of those approaches^{52,53,54,55} developed by Gyulassy-Levai-Vitev (GLV) based on an algebraic reaction operator formalism. The expansion parameter is the opacity $\chi = L/\lambda = \sigma\rho L$ of the system and the result is presented to all orders in powers of χ or equivalently to all twist parton-parton correlations. Other approaches relying on asymptotic techniques include BDMS^{56,57,58,59}, Z^{60,61,62,63}, and SW^{64,65,66,67} have been reviewed elsewhere⁶⁸. In the second part of this report the twist expansion approach^{69,70,71} for parton energy loss in nuclear matter is reviewed.

2.1. The GW Plasma Model

The GLV approach is built around a simple model of multiple scattering in a plasma formulated in GW⁷². However, the results of GLV^{52,53} are more general since even out of thermal equilibrium the effective in-medium interactions are of finite range $R \simeq \mu^{-1}$. Consider the sequential elastic

scattering of a high energy (jet) parton in the random color field produced by an ensemble of m static partons located at $\mathbf{x}_i = (z_i, \mathbf{x}_{\perp i})$ such that $z_{i+1} > z_i$ and $(z_{i+1} - z_i) \gg \mu^{-1}$, where μ is the color screening mass in the medium. As a simplified model of multiple scattering in a color neutral quark-gluon plasma, we assume a static Debye screened potential for each target parton:

$$V_i^a(\mathbf{q}) = g(T_i^a)_{c,c'} \frac{1}{\mathbf{q}^2 + \mu^2} e^{-i\mathbf{q}\cdot\mathbf{x}_i} , \quad (8)$$

where T_i^a is a d_i -dimensional generator of $SU(N)$ corresponding to the representation of the target parton at \mathbf{x}_i . The initial and final color indices, c, c' , which refer to the target parton, are averaged and summed over when computing the ensemble averaged cross sections. With $V_i^a \propto T_i^a$ the ensemble averaged potential vanishes everywhere, $\langle V_i^a \rangle \propto Tr T_i^a = 0$. However, since

$$Tr T_i^a T_j^b = \delta_{ab} \delta_{ij} (d_i/d_A) C_{2i} , \quad (9)$$

the diagonal mean square fluctuations and the cross sections are finite. Recall that for $SU(N)$ the second order Casimir, $C_{2i} = (N^2 - 1)/2N \equiv C_F$ for quarks in the fundamental ($d_i = N$) representation, while $C_{2i} = N \equiv C_A$ for gluons in the adjoint ($d_i = N^2 - 1 \equiv d_A$) representation.

In this potential, each scattering leads on the average to only a relatively small momentum transfer $q_i^\mu = (q_i^0, q_{zi}, \mathbf{q}_{\perp i})$ with each component being much less than the incident energy, E_0 . The assumption that the potentials are static is approximately valid in a high temperature plasma of massless quarks and gluons in the following sense: As $T \rightarrow \infty$, the effective coupling $g \rightarrow 0$ (albeit very slowly). The perturbative Debye screening mass $\mu \sim gT$ limits $q_{\perp} \lesssim gT$. The typical thermal energy $E_T \sim 3T$ of the plasma constituents is therefore large compared to μ . Consequently, the average energy loss per elastic collision, $-q^0 \approx -q^z \approx q_{\perp}^2/2E_T \propto g^2T$, is $\sim g$ times smaller than the average transverse momentum transfer.

Because we are interested in relatively low momentum transfer scattering ($\Lambda_{QCD} \ll q_{\perp} \sim gT \ll T$), the spin of the partons can be neglected. The jet parton is allowed, however, to be in an arbitrary d -dimensional representation of $SU(N)$ with generators, T^a , satisfying $T^a T^a = C_2 \mathbf{1}_d$.

The Born (color matrix) amplitude to scatter from an incident four momentum p_{i-1}^μ to p_i^μ in the potential centered at \mathbf{x}_i is then given by

$$M_i(p_i, p_{i-1}) = 2\pi \delta(p_i^0 - p_{i-1}^0) A_i(\mathbf{q}_i) e^{-i\mathbf{q}_i \cdot \mathbf{x}_i} , \quad (10)$$

*JET QUENCHING AND RADIATIVE ENERGY LOSS IN DENSE NUCLEAR MATTER*¹⁵

where $\mathbf{q}_i = \mathbf{p}_i - \mathbf{p}_{i-1}$, and A_i is shorthand for

$$A_i(\mathbf{q}_i) = T^a A_i^a(\mathbf{q}_i) = -2igE_0 T^a V_i^a(\mathbf{q}_i) . \quad (11)$$

The differential cross section averaged over initial and summed over final colors of both projectile and target partons reduces to the familiar form for low transverse momentum transfers:

$$d\sigma_i/dq_{\perp i}^2 \approx C_i \frac{4\pi\alpha^2}{(q_{\perp i}^2 + \mu^2)^2} , \quad (12)$$

where the color factor is

$$C_i = \frac{1}{dd_i} \text{Tr}(T^a T^b) \text{Tr}(T_i^a T_i^b) = C_2 C_{2i} / d_A . \quad (13)$$

For $SU(3)$, the number $2C_i$ gives the usual color factors $4/9, 1, 9/4$ for qq, qg, gg scattering respectively. In our notation, the angular distribution is given by

$$d\sigma_i/d\Omega_i = \frac{1}{dd_i} \text{Tr}|A_i(\mathbf{q}_i)|^2 / (4\pi)^2 . \quad (14)$$

2.2. GLV Formalism

In Refs.^{54,55} a systematic recursive graphical technique was developed and translated into an algebraic operator method. The goal was to compute medium induced gluon radiation amplitudes of the type shown in Fig. 12. The exponential growth of the number of graphs with the number of in-

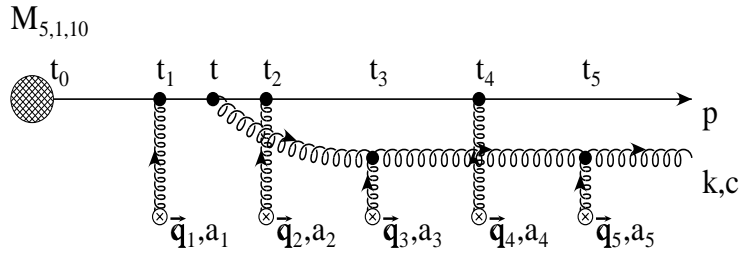


Fig. 12. Induced radiation amplitude⁵⁴ contributing to fifth order and higher orders in the opacity expansion of QCD energy loss in the GW model⁷². The crosses denote color screened Yukawa interactions on a scale μ . The blob is the initial hard jet amplitude.

interactions makes it very tedious to go beyond order three in opacity χ or twist 8 ($2 + 3 \times 2$) from the parton-parton correlations in the medium. In GLV^{52,53} the combinatorial problem is solved by summing the inclusive radiative gluon distributions recursively. The first step in the approach is to compute the three direct (single Born) and four surviving virtual (contact double Born) diagrams shown in Figs. 13 and 14 that contribute to the first order in opacity induced radiation. Detailed instructive calculation of these amplitudes is given in⁵².

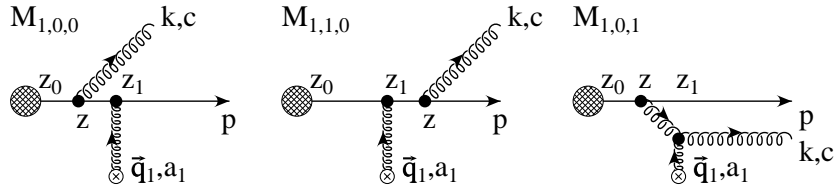


Fig. 13. Three first order (single Born) direct amplitudes that serve to define the \hat{D}_n component of the reaction operator in Eq.(21) are derived in Refs.^{52,53}.

For scattering of a jet off of n scattering centers located at depths z_i in a homogeneous medium of large area $\mu^2 A_\perp \gg 1$, we can write the inclusive radiative gluon “probability”, $P_n(\mathbf{k}, c)$, as a sum over products of partial sums of amplitudes and complementary complex conjugate amplitudes^{52,53}. Every term in the sum contributes to the same $\mathcal{O}(g^{4n+2})$ in the strong coupling constant g , where g^2 comes from the radiation vertex and $(g^4)^n$ is related to the n elastic scattering cross sections. The average value of n is the opacity, $\chi = \langle n \rangle = L/\lambda$, of the medium. It turns out surprisingly^{56,57} that λ is the mean free path of radiated gluons rather than the jet itself, as we shall show. The partial sums of diagrams at order n in the opacity expansion can be conveniently expressed in a tensor notation and constructed by repeated operations of $\hat{\mathbf{1}}$, \hat{D}_i , or \hat{V}_i corresponding to no, direct, or virtual interactions at scattering center i :

$$\mathcal{A}_{i_1 \dots i_n}(x, \mathbf{k}, c) = \prod_{m=1}^n \left(\delta_{0, i_m} + \delta_{1, i_m} \hat{D}_m + \delta_{2, i_m} \hat{V}_m \right) G_0(x, \mathbf{k}, c) . \quad (15)$$

Here G_0 is the initial hard $\{q, g\} + g$ color matrix amplitude, $x = k^+/p^+$ is the gluon lightcone momentum fraction, \mathbf{k} is the gluon transverse momentum, and c is its color index.

In the inclusive probability each class contracts with a unique comple-

JET QUENCHING AND RADIATIVE ENERGY LOSS IN DENSE NUCLEAR MATTER 17

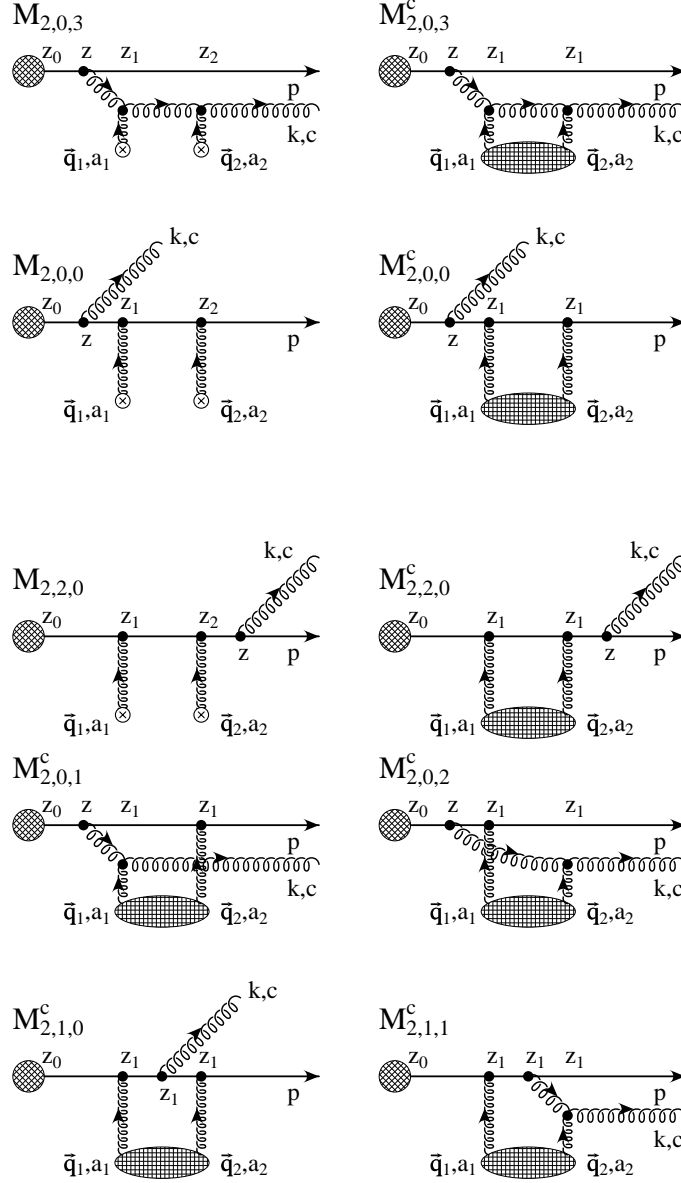


Fig. 14. Diagrams with two momentum exchanges that contribute to first and second orders in opacity. In the contact ($z_2 = z_1$) limit the (double Born) virtual (contact) amplitudes define the \hat{V}_n components of the reaction operator in Eq.(21)^{52,53}. Note that two of the diagrams vanish due to zero measure $\int_{z_1}^{z_1} dz \dots = 0$ of the radiation interval and two are topologically indistinct^{52,53}.

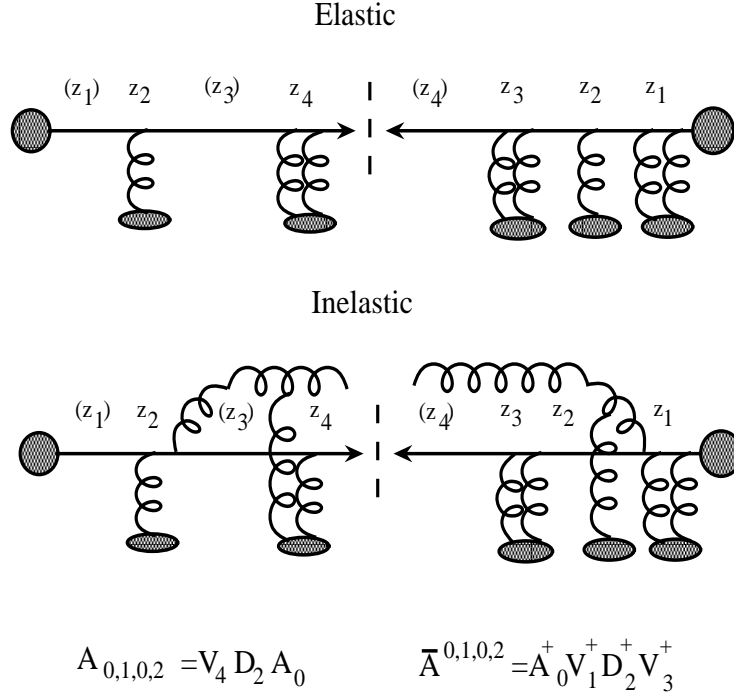


Fig. 15. Example of graphs constructed via \hat{D}_i, \hat{V}_i that contribute to the 4-th order in opacity (or twist 2+8 in-medium parton-parton correlations) in elastic and inclusive inelastic final state interactions. The longitudinal depths of active scattering centers are denoted by z_i and inactive (created with $\hat{1}_i$) by (z_i) . The form of \hat{D}_i, \hat{V}_i depend on the process type but the tensorial bookkeeping of partial sums of amplitudes is the same.

mentary class,

$$P_n(x, \mathbf{k}) = \bar{\mathcal{A}}^{i_1 \dots i_n}(x, \mathbf{k}, c) \mathcal{A}_{i_1 \dots i_n}(x, \mathbf{k}, c). \quad (16)$$

The complementary class is constructed to satisfy the fixed opacity power $\propto \chi^n$ requirement as

$$\bar{\mathcal{A}}^{i_1 \dots i_n}(x, \mathbf{k}, c) \equiv G_0^\dagger(x, \mathbf{k}, c) \prod_{m=1}^n \left(\delta_{0, i_m} \hat{V}_m^\dagger + \delta_{1, i_m} \hat{D}_m^\dagger + \delta_{2, i_m} \right). \quad (17)$$

Fig. 15 shows an example of how this formalism works at 4th order in opacity for elastic and inelastic inclusive distributions.

Detailed diagrammatic calculations that illustrate the color and kinematic modifications to the amplitudes for both direct and double Born momentum and color exchanges with the propagating jet+gluon system are given in Refs.^{52,53}. Direct single momentum transfer interactions enlarge rank $n - 1$ class elements as follows:

$$\begin{aligned} \hat{D}_n \mathcal{A}_{i_1 \dots i_{n-1}}(x, \mathbf{k}, c) &\equiv (a_n + \hat{S}_n + \hat{B}_n) \mathcal{A}_{i_1 \dots i_{n-1}}(x, \mathbf{k}, c) \\ &= a_n \mathcal{A}_{i_1 \dots i_{n-1}}(x, \mathbf{k}, c) + e^{i(\omega_0 - \omega_n)z_n} \mathcal{A}_{i_1 \dots i_{n-1}}(x, \mathbf{k} - \mathbf{q}_n, [c, a_n]) \\ &\quad - \left(-\frac{1}{2}\right)^{N_v(\mathcal{A}_{i_1 \dots i_{n-1}})} \mathbf{B}_n e^{i\omega_0 z_n} [c, a_n] T_{el}(\mathcal{A}_{i_1 \dots i_{n-1}}) , \end{aligned} \quad (18)$$

where $\mathbf{B}_n = \mathbf{H} - \mathbf{C}_n = \mathbf{k}/k^2 - (\mathbf{k} - \mathbf{q}_n)/(\mathbf{k} - \mathbf{q}_n)^2$ is the so-called Bertsch-Gunion amplitude for producing a gluon with transverse momentum \mathbf{k} in an isolated single collision with scattering center n . The momentum transfer to the jet is \mathbf{q}_n . The notation $\omega_n = (\mathbf{k} - \mathbf{q}_n)^2/2\omega$ is for a gluon with energy ω and a_n is the color matrix in the d_R dimensional representation of the jet with color Casimir C_R . $N_v = \sum_{m=1}^{n-1} \delta_{i_m, 2}$ counts the number of virtual interactions in $\mathcal{A}_{i_1 \dots i_{n-1}}$. $T_{el}(\mathcal{A}_{i_1 \dots i_{n-1}})$ is the elastic color factor associated with all $n - 1$ momentum transfers from the medium to the jet line.

Unitarity (virtual forward scattering) corrections to the direct processes involve the sum of four surviving double Born contact diagrams in Fig. 13 that enlarge rank $n - 1$ classes via the action of

$$\hat{V}_n = -\frac{1}{2}(C_A + C_R) - a_n \hat{S}_n - a_n \hat{B}_n = -a_n \hat{D}_n - \frac{1}{2}(C_A - C_R) . \quad (19)$$

This *key* operator relationship between direct and virtual insertions discovered in Refs.^{52,53} reduces the problem to recursive algebra. More specifically:

$$\begin{aligned} \hat{V}_n \mathcal{A}_{i_1 \dots i_{n-1}}(x, \mathbf{k}, c) &\equiv \left(-\frac{1}{2}(C_A + C_R) - a_n \hat{S}_n - a_n \hat{B}_n\right) \mathcal{A}_{i_1 \dots i_{n-1}}(x, \mathbf{k}, c) \\ &= -\frac{C_R + C_A}{2} \mathcal{A}_{i_1 \dots i_{n-1}}(x, \mathbf{k}, c) - e^{i(\omega_0 - \omega_n)z_n} a_n \mathcal{A}_{i_1 \dots i_{n-1}}(x, \mathbf{k} - \mathbf{q}_n, [c, a_n]) \\ &\quad - \left(-\frac{1}{2}\right)^{N_v} \frac{C_A}{2} \mathbf{B}_n e^{i\omega_0 z_n} c a_{n-1}^{i_{n-1}} \dots a_1^{i_1} . \end{aligned} \quad (20)$$

The tensorial bookkeeping of classes of diagrams makes it possible to construct the distribution of radiated gluons in the case of n interactions,

$P_n(x, \mathbf{k})$, recursively from lower rank (opacity) classes via a “reaction” operator

$$P_n = \bar{\mathcal{A}}^{i_1 \dots i_{n-1}} \hat{R}_n \mathcal{A}_{i_1 \dots i_{n-1}}, \quad \hat{R}_n = \hat{D}_n^\dagger \hat{D}_n + \hat{V}_n + \hat{V}_n^\dagger. \quad (21)$$

Using the key identity (19), the reaction matrix simplifies to

$$\hat{R}_n = (\hat{D}_n - a_n)^\dagger (\hat{D}_n - a_n) - C_A = (\hat{S}_n + \hat{B}_n)^\dagger (\hat{S}_n + \hat{B}_n) - C_A.$$

The next major simplification occurs because both \hat{S} and \hat{B} involve the same gluon color rotation through if^{cad} . This fact reduces the color algebra to simple multiplicative Casimir factors in the adjoint representation

$$\begin{aligned} \bar{\mathcal{A}}^{i_1 \dots i_{n-1}} (\hat{S}_n^\dagger \hat{S}_n - C_A) \mathcal{A}_{i_1 \dots i_{n-1}} &= C_A (P_{n-1}(\mathbf{k} - \mathbf{q}_n) - P_{n-1}(\mathbf{k})) \\ &= C_A (e^{i\mathbf{q}_n \cdot \hat{\mathbf{b}}} - 1) P_{n-1}(\mathbf{k}), \end{aligned} \quad (22)$$

where $\hat{\mathbf{b}} = i\nabla_{\mathbf{k}}$ is the transverse momentum shift operator. We have proved in Refs.^{52,53} that

$$\bar{\mathcal{A}}^{i_1 \dots i_{n-1}} \hat{B}_n^\dagger \hat{B}_n \mathcal{A}_{i_1 \dots i_{n-1}} = 0. \quad (23)$$

The interference term is also found to be color trivial (containing only powers of the Casimir in the adjoint representation C_A) and can be expressed in recursive form:

$$2\text{Re} \bar{\mathcal{A}}^{i_1 \dots i_{n-1}} \hat{B}_n^\dagger \hat{S}_n \mathcal{A}_{i_1 \dots i_{n-1}} = -2C_A \mathbf{B}_n \cdot \left(\text{Re} e^{-i\omega_n z_n} e^{i\mathbf{q}_n \cdot \hat{\mathbf{b}}} \mathbf{I}_{n-1} \right). \quad (24)$$

Eqs.(22)–(24) present a clear proof that only the gluon mean free path which is proportional to C_A (or equivalently the gluon elastic scattering cross section) appears in the induced non-Abelian bremsstrahlung formulas.

The transverse vector amplitude \mathbf{I}_n above obeys a recursion relation

$$\mathbf{I}_n = C_A \left(e^{i(\omega_0 - \omega_n) z_n} e^{i\mathbf{q}_n \cdot \hat{\mathbf{b}}} - 1 \right) \mathbf{I}_{n-1} - \delta_{n,1} C_A C_R \mathbf{B}_1 e^{i\omega_0 z_1}, \quad (25)$$

where $\mathbf{I}_0 = -C_R \mathbf{H} e^{i\omega_0 z_0}$, and the Gunion-Bertsch amplitude can be written as

$$\mathbf{B}_1 e^{i\omega_0 z_1} = - \left(e^{i(\omega_0 - \omega_1) z_1} e^{i\mathbf{q}_1 \cdot \hat{\mathbf{b}}} - 1 \right) \mathbf{H} e^{i\omega_0 z_1}. \quad (26)$$

For $n \geq 1$ Eq.(25) can be solved in closed form

$$\mathbf{I}_n = C_R C_A^n \left[\prod_{m=1}^n \left(e^{i(\omega_0 - \omega_m) z_m} e^{i\mathbf{q}_m \cdot \hat{\mathbf{b}}} - 1 \right) \right] \mathbf{H} (e^{i\omega_0 z_1} - e^{i\omega_0 z_0}), \quad (27)$$

where the product is understood as ordered from left to right in decreasing order in operators labeled by m .

JET QUENCHING AND RADIATIVE ENERGY LOSS IN DENSE NUCLEAR MATTER 21

The inclusive radiation “probability” is then found to obey the soluble recursion relation

$$P_n(\mathbf{k}) = C_A(P_{n-1}(\mathbf{k} - \mathbf{q}_n) - P_{n-1}(\mathbf{k})) - 2C_A \mathbf{B}_n \cdot \left(\mathbf{Re} e^{-i\omega_n z_n} e^{i\mathbf{q}_n \cdot \hat{\mathbf{b}}} \mathbf{I}_{n-1} \right) + \delta_{n,1} C_A C_R |\mathbf{B}_1|^2 . \quad (28)$$

The initial condition for this recursion relation is the initial hard vertex radiation amplitude without final state interactions that is given by $P_0 = C_R \mathbf{H}^2 = C_R / \mathbf{k}^2$.

The solution to the problem for any order n in multiparticle interactions can therefore be expressed in closed form as

$$P_n(\mathbf{k}) = -2C_R C_A^n \mathbf{Re} \sum_{i=1}^n \left\{ \prod_{j=i+1}^n (e^{i\mathbf{q}_j \cdot \hat{\mathbf{b}}} - 1) \right\} \otimes \mathbf{B}_i \cdot e^{i\mathbf{q}_i \cdot \hat{\mathbf{b}}} e^{-i\omega_0 z_i} \times \left\{ \prod_{m=1}^{i-1} (e^{i(\omega_0 - \omega_m) z_m} e^{i\mathbf{q}_m \cdot \hat{\mathbf{b}}} - 1) \right\} \otimes \mathbf{H}(e^{i\omega_0 z_1} - e^{i\omega_0 z_0}) . \quad (29)$$

This expression is very general and is suitable for any distribution of interaction centers as well as any distribution of z_i dependent transverse momenta exchanges that can arise due to expansion of the medium. Therefore, it can be directly applied to realistic expanding plasmas where the distance between adjacent centers (the mean free path) varies along the medium as does the local screening scale, $\mu(z)$. This form is also well suited for possible future Monte Carlo implementation for arbitrary \mathbf{q}_i, z_i medium ensemble averages.

The final complete solution to the inclusive induced gluon radiation valid to *all* orders in opacity can be expressed in terms of the following infinite series:

$$x \frac{dN^g}{dx d^2\mathbf{k}} = \frac{C_R \alpha_s}{\pi^2} \sum_{n=1}^{\infty} \frac{1}{n!} \prod_{i=1}^n \left(\int_{z_{i-1}}^{\infty} dz_i \int d^2\mathbf{q}_i \left[\frac{d^2\sigma_g(z_i)}{d^2\mathbf{q}_i} - \sigma_g(z_i) \delta^2(\mathbf{q}_i) \right] \right) \times \rho_n(z_1, \dots, z_n) \left(-2 \mathbf{C}_{(1, \dots, n)} \cdot \sum_{m=1}^n \mathbf{B}_{(m+1, \dots, n)(m, \dots, n)} \times \left[\cos \left(\sum_{k=2}^m \omega_{(k, \dots, n)} \Delta z_k \right) - \cos \left(\sum_{k=1}^m \omega_{(k, \dots, n)} \Delta z_k \right) \right] \right) , \quad (30)$$

where $\sum_2^1 \equiv 0$ is understood. The notation is defined as follows:

$$\begin{aligned} \mathbf{H} &= \frac{\mathbf{k}}{\mathbf{k}^2}, & \mathbf{C}_{(i_1 i_2 \dots i_m)} &= \frac{(\mathbf{k} - \mathbf{q}_{i_1} - \mathbf{q}_{i_2} - \dots - \mathbf{q}_{i_m})}{(\mathbf{k} - \mathbf{q}_{i_1} - \mathbf{q}_{i_2} - \dots - \mathbf{q}_{i_m})^2}, \\ \mathbf{B}_i &= \mathbf{H} - \mathbf{C}_i, & \mathbf{B}_{(i_1 i_2 \dots i_m)(j_1 j_2 \dots j_n)} &= \mathbf{C}_{(i_1 i_2 \dots i_m)} - \mathbf{C}_{(j_1 j_2 \dots j_n)} \\ \omega_{(m, \dots, n)} &= \frac{(\mathbf{k} - \mathbf{q}_m - \dots - \mathbf{q}_n)^2}{2xE}. \end{aligned} \quad (31)$$

The infinite opacity series can be understood as a sum over *all twist* parton-parton correlations, $\langle \dots (2n FF) \dots \rangle$, in the nuclear matter. We emphasize that Eq.(30) is not restricted to uncorrelated geometries as in Refs.^{56–66}. It also allows the inclusion of finite kinematic boundaries on the \mathbf{q}_i as well as different functional forms and elastic cross sections $\sigma_g(i)$ along the eikonal path. The first and second orders in opacity (twists $2 + 2$, $2 + 4$) have also been checked^{52,53} through explicit calculations of the corresponding direct and virtual cut diagrams. The $\sum_i \mathbf{q}_i = \mathbf{k}$ divergences, naively present in the propagators $\mathbf{C}_{(i_1 i_2 \dots i_m)}$, $\mathbf{B}_{(i_1 i_2 \dots i_m)(j_1 j_2 \dots j_n)}$ in Eq.(30), are canceled by the interferences phases $\omega_{(m, \dots, n)}$. Eq.(30) also provides further insight in the LPM effect in QCD at a microscopic/diagrammatic level by keeping track of the destructive interference among all pairs of amplitudes to all orders in opacity.

For particular models of the target geometry one can proceed further analytically. For a homogeneous rectangular geometry, the average over the longitudinal target profile with

$$\rho_n(z_1, \dots, z_n) = n! \rho_0^n \theta(L - z_n) \theta(z_n - z_{n-1}) \dots \theta(z_2 - z_1), \quad (32)$$

where the mean density is $\rho_0 = N_s/LA_\perp$, leads to an oscillatory pattern that is an artifact of the assumed sharp edges. Here A_\perp is the transverse area of the interaction region and N_s is the total number of scattering centers. A somewhat more realistic model may be an exponential longitudinal distribution of scattering center separations

$$\rho_n(z_1, \dots, z_n) = \prod_{j=1}^n \frac{\theta(\Delta z_j) N_s}{L_e(n) A_\perp} e^{-\Delta z_j / L_e(n)}. \quad (33)$$

This converts the oscillating formation phase factors in Eq.(30) into Lorentzian factors

$$\int d\rho_n \cos \left(\sum_{k=j}^m \omega_{(k, \dots, n)} \Delta z_k \right) = \frac{N_s^n}{A_\perp^n} \text{Re} \prod_{k=j}^m \frac{1}{1 + i\omega_{(k, \dots, n)} L_e(n)}. \quad (34)$$

JET QUENCHING AND RADIATIVE ENERGY LOSS IN DENSE NUCLEAR MATTER 23

In order to fix $L_e(n)$, we can impose $\langle z_k - z_0 \rangle = kL/(n+1)$. This constrains^{52,53,54} $L_e(n) = L/(n+1)$.

2.3. First Order Non-Abelian Energy Loss

The simplest and fortunately dominant (a *posteriori*) application^{52,53} of our general solution to the energy loss problem was to calculate numerically the total radiated energy loss as a function of jet energy E , plasma depth L , and the typical transverse momentum transfer μ . In the absence of a medium, the gluon radiation associated with the parton jet (in the small x approximation, where we do not distinguish between quark and gluon parents) is distributed as

$$x \frac{dN^{(0)}}{dx d\mathbf{k}^2} = \frac{C_R \alpha_s}{\pi} \frac{1}{\mathbf{k}^2}, \quad (35)$$

where $x = k^+/E^+ \approx \omega/E$, and C_R is the Casimir of the jet in the d_R -dimensional color representation. The differential energy distribution outside a cone defined by $\mathbf{k}^2 > \mu^2$ is given by

$$\frac{dI^{(0)}}{dx} = \frac{2C_R \alpha_s}{\pi} E \log \frac{|\mathbf{k}|_{\max}}{\mu}, \quad (36)$$

where the upper kinematic limit is $\mathbf{k}_{\max}^2 = \min[4E^2 x^2, 4E^2 x(1-x)]$. The energy loss outside the cone in the vacuum is then given by

$$\Delta E^{(0)} = \frac{2C_R \alpha_s}{\pi} E \log \frac{E}{\mu}. \quad (37)$$

Beyond the small x approximation, the splitting functions $P_{gq}(x)$ and $P_{gg}(x)$ can give rise to some small corrections. While Eq.(37) overestimates the radiative energy loss in the vacuum (self-quenching), it is important to note that $\Delta E^{(0)}/E \sim 50\%$ is typically much larger than the medium induced energy loss. However, the vacuum energy loss is included in the DGLAP evolution of the fragmentation functions $D_{h/c}(z, Q^2)$.

To compute the medium induced radiation we focus on the density of the N_s scattering centers given by Eq.(33). Averaging over the momentum transfer \mathbf{q}_1 via the color Yukawa potential leads to a very simple first order opacity result for the $x \ll 1$ gluon double differential distribution

$$x \frac{dN^{(1)}}{dx d\mathbf{k}^2} = x \frac{dN^{(0)}}{dx d\mathbf{k}^2} \frac{L}{\lambda_g} \int_0^{q_{\max}^2} d^2 \mathbf{q}_1 \frac{\mu_{eff}^2}{\pi(\mathbf{q}_1^2 + \mu^2)^2} \times \frac{2 \mathbf{k} \cdot \mathbf{q}_1 (\mathbf{k} - \mathbf{q}_1)^2 L^2}{16x^2 E^2 + (\mathbf{k} - \mathbf{q}_1)^4 L^2}, \quad (38)$$

where the opacity factor $L/\lambda_g = N_s \sigma_{el}^{(g)}/A_\perp$ arises from the sum over the N_s distinct targets. Note that the radiated gluon mean free path $\lambda_g = (C_A/C_R)\lambda$ appears rather than the jet mean free path. The upper kinematic bound on the momentum transfer is $q_{\max}^2 = s/4 \simeq 3E\mu$ and $1/\mu_{eff}^2 = 1/\mu^2 - 1/(\mu^2 + q_{\max}^2)$. For SPS and RHIC energies this finite limit cannot be ignored. Numerical results comparing the first three orders in opacity corrections to the hard distribution Eq.(35) were presented in Refs.^{52,53} and the opacity series was shown to converge fast is dominated by its first order term for realistic nuclear opacities. Fig. 16 illustrates the convergence properties of Eq.(30) in the example of the mean energy loss ΔE , as well as the quadratic dependence of ΔE on the size of the nuclear matter for static media.

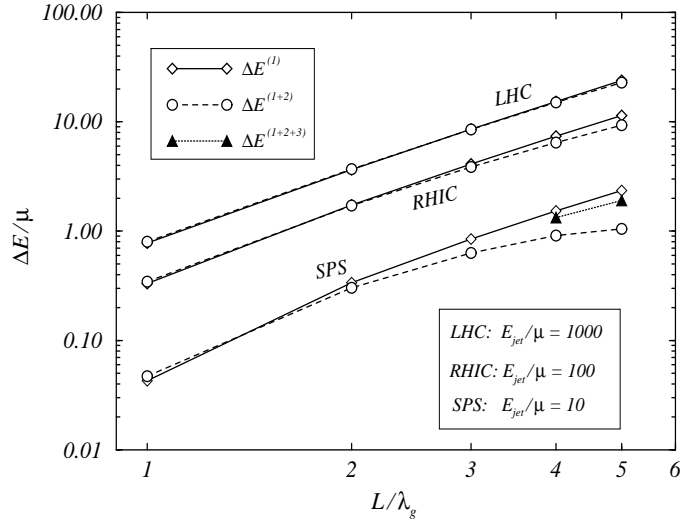


Fig. 16. The radiative energy loss of a quark jet with energy $E_{jet} = 5, 50, 500$ GeV (at SPS, RHIC, LHC) is plotted as a function of the opacity L/λ_g ($\lambda_g = 1$ fm, $\mu = 0.5$ GeV) for a static medium from Ref.^{52,53}. Solid curves show the first order in opacity results. The dashed curves show results up to second order in opacity, and two third order results are shown by solid triangles for SPS energies.

In Ref.⁷³ we considered various asymptotic limits of the first order energy loss in 1+1D and 1+3D expanding plasmas. In the case that the mean density decreases as

$$\rho(z = \tau) = \rho_0 \left(\frac{\tau_0}{\tau} \right)^\alpha \quad (39)$$

JET QUENCHING AND RADIATIVE ENERGY LOSS IN DENSE NUCLEAR MATTER 25

due to a longitudinal Bjorken expansion, it is possible to obtain a closed analytic formula³⁶ under the strong assumption that no kinematic bounds need to be considered. For a hard jet penetrating the quark-gluon plasma,

$$\frac{d\Delta E^{(1)}}{dx} = \frac{2C_R\alpha_s}{\pi} E \int_{\tau_0}^{\infty} \frac{d\tau}{\lambda(\tau)} f(Z(x, \tau)), \quad (40)$$

where $x \simeq \omega/E$ is the momentum fraction of the radiated gluon and the formation physics function $f(Z(x, \tau))$ is defined³⁶ to be

$$f(x, \tau) = \int_0^{\infty} \frac{du}{u(1+u)} [1 - \cos(uZ(x, \tau))] . \quad (41)$$

With $Z(x, \tau) = (\tau - \tau_0)\mu^2(\tau)/2xE$ as the local formation physics parameter, two simple analytic limits of Eq.(41) can be obtained. For $x \gg x_c = \mu(\tau_0)^2\tau_0^{\frac{2\alpha}{3}}L^{1-\frac{2\alpha}{3}}/2E = L\mu^2(L)/2E$, in which case the formation length is large compared to the size of the medium, the small $Z(x, \tau)$ limit applies, leading to $f(Z) \approx \pi Z/2$. The interference pattern along the gluon path becomes important and accounts for the non-trivial dependence of the energy loss on L . When $x \ll x_c$, i.e. the formation length is small compared to the plasma thickness, one gets $f(Z) \approx \log Z$. In the $x \gg x_c$ limit³⁶, the radiative spectrum Eq.(40) becomes

$$\frac{d\Delta E_{x \gg x_c}^{(1)}}{dx} \approx \frac{C_R\alpha_s}{2(2-\alpha)} \frac{\mu(\tau_0)^2\tau_0^\alpha L^{2-\alpha}}{\lambda(\tau_0)} \frac{1}{x} . \quad (42)$$

In the opposite $x \ll x_c$ limit we have

$$\frac{d\Delta E_{x \ll x_c}^{(1)}}{dx} \approx \frac{6C_R\alpha_s}{\pi(3-\alpha)} E \frac{\tau_0^{\frac{\alpha}{3}} L^{1-\frac{\alpha}{3}}}{\lambda(\tau_0)} \log \frac{\mu(\tau_0)^2\tau_0^{\frac{2\alpha}{3}} L^{1-\frac{2\alpha}{3}}}{2xE} \quad (43)$$

and the intensity spectrum has an integrable divergence at $x = 0$. Higher orders in opacity do change the x -dependence of the radiative spectrum relative to Eqs.(42) and (43), but this change is small^{52,53} for $L \sim R_A \simeq 5$ fm.

The mean energy loss (to first order in χ) integrates to

$$\Delta E^{(1)} = \frac{C_R\alpha_s}{2(2-\alpha)} \frac{\mu(\tau_0)^2\tau_0^\alpha L^{2-\alpha}}{\lambda(\tau_0)} \left(\log \frac{2E}{\mu(\tau_0)^2\tau_0^{\frac{2\alpha}{3}} L^{1-\frac{2\alpha}{3}}} + \dots \right) . \quad (44)$$

The logarithmic enhancement with energy comes from the $x_c < x < 1$ region^{52,53}. In the case of sufficiently large jet energies ($E \rightarrow \infty$) this term dominates. For parton energies < 20 GeV, however, corrections to this leading $\log 1/x_c$ expression that can be exactly evaluated numerically from

the GLV expression and are found to be comparable in size. The effective $\Delta E/E$ in this energy range is approximately constant.

In order to study non-central collisions and azimuthal anisotropy we also solved the analytically tractable case of a sharp expanding elliptic cylinder. We approximate the assumed ϕ_0 independent screening $\mu(\tau) \approx gT(\tau) = 2(\rho(\tau)/2)^{1/3}$ since $g \simeq 2$ and $\rho = (16\zeta(3)/\pi^2)T^3 \simeq 2T^3$ for a gluon plasma. We define $\tau(\phi_0)$ as the escape time for the jet to reach the expanding elliptic surface from an initial point $\mathbf{x}_0 = (x_0, y_0)$ in the azimuthal direction ϕ_0 :

$$\frac{(x_0 + \tau \cos \phi_0)^2}{(R_x + v_x \tau)^2} + \frac{(y_0 + \tau \sin \phi_0)^2}{(R_y + v_y \tau)^2} = 1 . \quad (45)$$

We take $\omega(\phi_0) = 2\tau(\phi_0)(\rho(\tau(\phi_0))/2)^{2/3}$ to estimate an upper bound on the logarithmic enhancement factor. Performing the remaining integrals one gets:

$$\begin{aligned} \Delta E^{(1)}(\phi_0) &\approx \frac{9C_R \alpha_s^3}{4} \frac{dN^g}{dy} \log \frac{E}{\omega(\phi_0)} \int_0^\infty d\tau \frac{1}{R_x + v_x \tau} \frac{1}{R_y + v_y \tau} \\ &\quad \times \theta \left(1 - \frac{(x_0 + \tau \cos \phi_0)^2}{(R_x + v_x \tau)^2} + \frac{(y_0 + \tau \sin \phi_0)^2}{(R_y + v_y \tau)^2} \right) \\ &= \frac{9}{4} \frac{C_R \alpha_s^3}{R_x R_y} \frac{dN^g}{dy} \frac{\log \frac{1+a_x \tau(\phi_0)}{1+a_y \tau(\phi_0)}}{a_x - a_y} \log \frac{E}{\omega(\phi_0)} , \end{aligned} \quad (46)$$

where $a_x = v_x/R_x$, $a_y = v_y/R_y$. This expression provides a simple analytic generalization that interpolates between a pure Bjorken 1+1D expansion for small $a_{x,y}\tau$, and a 3+1D expansion at large $a_{x,y}\tau$.

In the special case of a pure Bjorken (longitudinal) expansion with $v_x = v_y = 0$,

$$\Delta E_{Bj}^{(1)}(\phi_0) = \frac{9C_R \alpha_s^3}{4R_x R_y} \frac{dN^g}{dy} \tau(\phi) \log \frac{E}{\omega(\phi_0)} . \quad (47)$$

In this case, the energy loss depends *linearly* on $\tau(\phi)$.

2.4. Centrality and Rapidity Dependence of the Cronin Effect at RHIC

In the subsections that follow we will describe some of the important applications/predictions of the GLV reaction operator formalism to initial and final state multiparton interactions. We emphasize that these calculations can provide complementary information about the properties of cold and hot nuclear matter such as the transport coefficients μ^2/λ_q , μ^2/λ_g and the

JET QUENCHING AND RADIATIVE ENERGY LOSS IN DENSE NUCLEAR MATTER 27

effective initial gluon number density and energy density created in relativistic heavy ion reactions.

In Refs.^{40,74} the explicit solution for the transverse momentum distribution of partons that have traversed cold nuclear matter has been found using the GLV approach:

$$\frac{d^3 N^f(k_{\parallel}, \mathbf{k}_{\perp})}{dk_{\parallel} d^2 \mathbf{k}_{\perp}} = \sum_{n=0}^{\infty} \frac{\chi^n}{n!} \int \prod_{i=1}^n d^2 \mathbf{q}_{i\perp} \left[\frac{1}{\sigma_{el}} \frac{d\sigma_{el}(R, T)}{d^2 \mathbf{q}_{i\perp}} \times \left(e^{-\mathbf{q}_{i\perp} \cdot \vec{\nabla}_{\mathbf{k}_{\perp}}} \otimes e^{-q_{i\parallel} \partial_{k_{\parallel}}} - 1 \right) \right] \times \frac{d^3 N^i(k_{\parallel}, \mathbf{k}_{\perp})}{dk_{\parallel} d^2 \mathbf{k}_{\perp}} . \quad (48)$$

This leads to nuclear induced broadening $\langle \Delta k_{\perp}^2 \rangle_{pA} = \mu^2 \chi \xi$ for opacity $\chi = \langle L \rangle / \lambda$ and typical transverse momentum squared μ^2 . Beyond the naive Gaussian approximation harder fluctuations along the projectile path lead to a logarithmic enhancement $\langle \Delta k_{\perp}^2 \rangle_{pA}$, i.e. $\xi = \ln(1 + c p_T^2)$. The question of the effective longitudinal momentum shift associated with this broadening has also been addressed^{40,74}:

$$-\Delta k_{\parallel} = \mu^2 \chi \xi \frac{1}{2k_{\parallel}} . \quad (49)$$

To implement *initial state* elastic and radiative energy loss we focus on the large $Q^2 \simeq p_T^2$ partonic subprocess $a + b \rightarrow c + d$, where k_a, k_b are the initial momenta involved in the hard part $d\sigma/dt$ of Eq.(3). If partons a and b have lost fractions ϵ_{α} ($\alpha = a, b$) of their longitudinal momenta according to a probability distributions $P_{\alpha}(\epsilon)$, then $\tilde{k}_{\alpha} = k_{\alpha}/1 - \epsilon_{\alpha}$ and

$$f_{\alpha/p}(x_{\alpha}, Q^2) \rightarrow \int d\epsilon_{\alpha} P_{\alpha}(\epsilon_{\alpha}) f_{\alpha/p} \left(\tilde{x}_{\alpha} = \frac{x}{1 - \epsilon_{\alpha}}, Q^2 \right) \theta(\tilde{x}_{\alpha} \leq 1) , \quad (50)$$

at asymptotic $t = -\infty$. Eq.(50) provides a simple modification to the factorized pQCD hadron production formalism. For bremsstrahlung processes, $P_{\alpha}(\epsilon)$ are sensitive to multiple gluon emission⁴⁷. For the simpler case where one considers only the mean energy loss, $P(\epsilon) = \delta(\epsilon - \langle \Delta k_0 \rangle / k_0)$. More specifically, for the elastic longitudinal shift that we consider here, $P_{\alpha}(\epsilon) = \delta \left(\epsilon - \mu^2 \chi_{\alpha} \xi / 2k_{\alpha\parallel} \right)$ and

$$f_{\alpha/p}(x_{\alpha}, Q^2) \rightarrow f_{\alpha/p} \left(x_{\alpha} + \frac{\mu^2 \chi_{\alpha} \xi}{x_{\alpha}} \frac{2}{s}, Q^2 \right) \theta(\tilde{x}_{\alpha} \leq 1) . \quad (51)$$

The observable effects of Eqs.(50) and (51) can be very different for valence quarks, sea quarks, and gluons due to the different x -dependence of the PDFs.

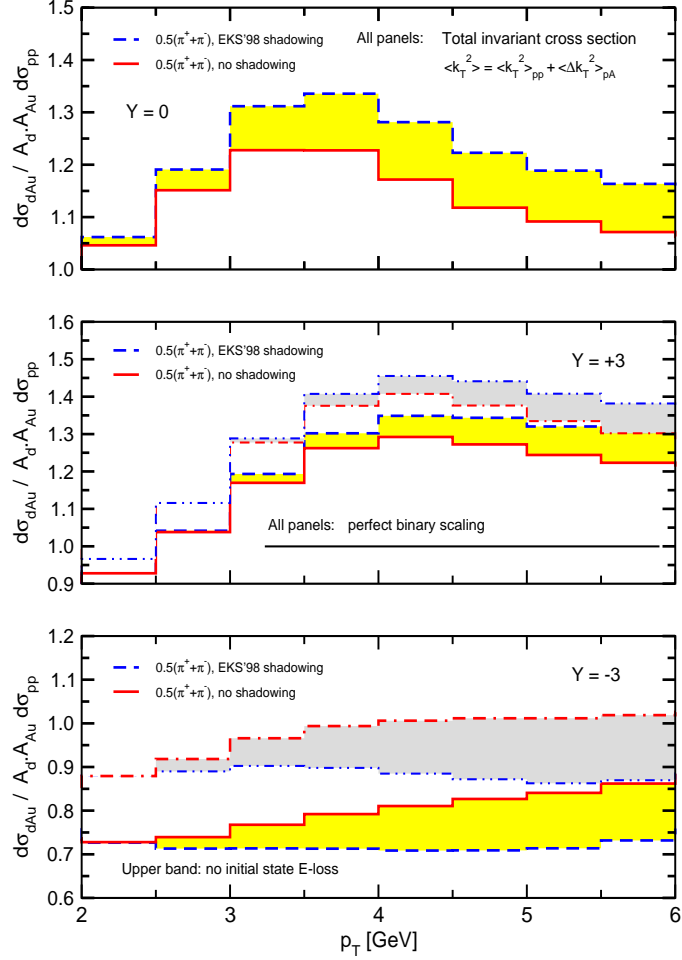


Fig. 17. Rapidity dependence of the Cronin effect in $d + Au$ reactions at $\sqrt{s_{NN}} = 200$ GeV with and without antishadowing or EMC effect from Ref.⁴⁰. The result of switching off elastic energy loss is also shown via the upper bands for $y = \pm 3$.

A natural application of these results is in the quantitative description of the Cronin effect. Perturbative calculations that include initial state parton broadening remain its only successful explanation to date^{39,40,75,76,77,78}. Comparison to low energy data on proton-nucleus collisions^{40,75} allows

JET QUENCHING AND RADIATIVE ENERGY LOSS IN DENSE NUCLEAR MATTER 29

us to extract the transport coefficients of cold nuclear matter, $\mu^2/\lambda_q = 0.06 \text{ GeV}^2/\text{fm}$ and $\mu^2/\lambda_g = 0.14 \text{ GeV}^2/\text{fm}$. These estimates include the effective elastic initial state energy loss and are $\sim 25\%$ bigger relative to the case when the longitudinal momentum shifts have been neglected^{75,79}. The transport coefficients of cold nuclear matter change only slightly⁴⁰ with \sqrt{s} and can be used to predict the centrality and rapidity dependence of the Cronin effect in $d + Au$ reactions at RHIC.

Fig. 17 shows the computed rapidity dependence of the Cronin effect in $d + Au$ reactions at RHIC. At midrapidity, $y = 0$, in the computed transverse momentum range, we find slight Cronin enhancement $R_{dAu \text{ max}} = 1.2$ relative to the binary collision scaled $p + p$ result even with initial state elastic energy loss. Including strong antishadowing (shown with dashed lines) leads to $R_{dAu \text{ max}} = 1.3$. The effect of antishadowing becomes increasingly important at higher p_T . Experiments at RHIC can thus help constrain the poorly known nuclear modification to the PDFs for gluons. At forward $y = +3$ rapidity (in the direction of the deuteron beam) the Cronin intercept ($R_{dAu} = 1$) and maximum $R_{dAu \text{ max}}$ are both shifted to slightly higher p_T . The most distinct prediction at forward rapidities is the significantly larger Cronin enhancement region extending to high p_T . This is understood in terms of the softening of the hadron spectra away from midrapidity, as predicted by perturbative QCD. Steeper spectra tend to enhance the effect of otherwise identical transverse momentum kicks. At backward $y = -3$ rapidity there is no enhancement since the nucleus does not scatter multiply on the deuteron. This region is shown to be sensitive to the initial state energy loss⁴⁰. For further details on the systematic understanding of the Cronin effect versus \sqrt{s} the reader is referred to Refs.^{75,76}. Recently it has been suggested by models based on gluon saturation, final state hadron absorption, and coherent nucleon scattering, that hadron cross sections in $d + Au$ reactions will be suppressed by about 30% for charged hadrons relative to the binary collision scaled $p + p$ result. Experimental data at RHIC will make possible a critical test of the validity of different theoretical models.

2.5. Jet Tomography of $d + Au$ and $Au + Au$ at SPS, RHIC, and LHC

Some of the most important applications^{47,75} of the GLV results on medium induced gluon bremsstrahlung are related to jet tomography, the study of the properties of matter through the attenuation pattern of fast

particles that propagate and lose energy as a result of multiple elastic and inelastic scatterings. Under the assumption of local thermal equilibrium all relevant scales in the problem, such as the Debye screening scale μ , can be related to dN^g/dy – the initial effective gluon rapidity density of the bulk soft background matter (the quark-gluon plasma).

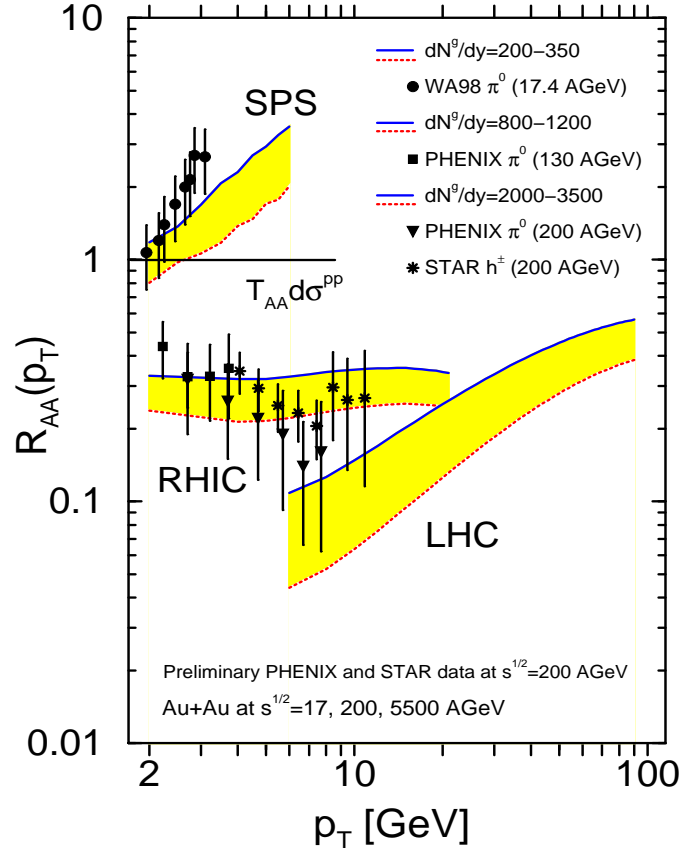


Fig. 18. The suppression/enhancement ratio $R_{AA}(p_T)$ ($A = B = Au$) for neutral pions at $\sqrt{s_{NN}} = 17, 200, 5500$ GeV from Ref.⁷⁵. Solid (dashed) lines correspond to the smaller (larger) effective initial gluon rapidity densities at given \sqrt{s} that drive parton energy loss. Data on π^0 production in central $Pb + Pb$ at $\sqrt{s_{NN}} = 17.4$ GeV from WA98²⁴ and in central $Au + Au$ at $\sqrt{s_{NN}} = 130$ GeV, as well as *preliminary* data at 200 GeV from PHENIX^{3,1} and h^\pm central/peripheral data from STAR⁵ are shown. The sum of estimated statistical and systematic errors is indicated.

JET QUENCHING AND RADIATIVE ENERGY LOSS IN DENSE NUCLEAR MATTER 31

Our main results for central $Au + Au$ reactions, which includes three important nuclear effects, Cronin+Shadowing+Quenching, are presented in Fig. 18. Jet tomography consists of determining the effective initial gluon rapidity density dN^g/dy that best reproduces the quenching pattern of the data^{1,3,5,24}. At SPS the large Cronin enhancement⁷⁵ is reduced by a factor of two with $dN^g/dy = 350$ but the data are more consistent with a smaller gluon density ≤ 200 . Unfortunately at this low energy the results are very sensitive to the details of the model. At RHIC, for $p_T > 2$ GeV jet quenching dominates, but surprisingly the rate of variation with p_T of the Cronin enhancement and jet quenching conspire to yield an approximately constant suppression pattern with magnitude dependent only on the initial dN^g/dy . At higher $p_T > 20$ GeV the softening of the initial jet spectra due to the EMC modification of the PDFs compensates for the reduced energy loss. This unexpected interplay among the three nuclear effects at RHIC was our main prediction in Ref.⁷⁵. Preliminary $\sqrt{s} = 200$ AGeV PHENIX and STAR results included in Fig. 18 support the predicted magnitude and approximate p_T dependence of the suppression. At LHC energies the much larger gluon densities $dN^g/dy \sim 2000 - 3500$ are expected to lead to a dramatic variation of quenching with p_T , as shown. In nuclear media of high opacity the mean fractional energy loss $\langle \Delta E \rangle / E$ of moderately hard partons can become of the order of unity. For LHC this may be reflected in the $p_T \leq 10$ GeV region through deviations from the extrapolated high- p_T suppression trend. Hadronic fragments coming from energetic jets would tend to compensate the rapidly increasing quenching with decreasing transverse momentum (seen in Fig. 18) and may restore the hydrodynamic-like participant scaling in the soft regime.

2.6. Enhanced Baryon/Meson Ratios

One of the unexpected results reported during the first year RHIC run at $\sqrt{s_{NN}} = 130$ GeV was that, in contrast to the strong π^0 quenching for $2 \text{ GeV} < p_T < 5 \text{ GeV}$, the corresponding charged hadrons were found to be suppressed by only a factor $\sim 2 - 2.5$. Even more surprisingly, the identified particle spectra analysis suggests that $R_B(p_T) = \bar{p}/\pi^-, p/\pi^+ \geq 1$ for $p_T > 2 \text{ GeV}$. Thus, baryon and antibaryon production may in fact dominate the moderate to high p_T hadron flavor yields^{80,81,82,83}. These and other data point to a possible novel baryon transport dynamics nucleus-nucleus reactions. More recent results corroborate the non-perturbative baryon production hypothesis through equally abundant Λ and $\bar{\Lambda}$ production^{84,85}. It

has also been observed that the mean transverse momentum $\langle p_T \rangle_B$ for various baryon and antibaryon species is approximately constant and deviates from the common hydrodynamic flow systematics of soft hadron production in $A + A$ collisions. Identified particle analyses from the recent $\sqrt{s_{NN}} = 200$ GeV RHIC run find similar puzzling features of moderate- p_T baryon spectra^{3,4,5}.

In Refs.^{86,87,88} the GLV jet energy loss^{52,53} was combined with a topological non-perturbative baryon production and transport mechanism^{89–93} to gain insight into the anomalous anti-baryon behavior at RHIC. Phenomenological applications are currently based on Regge theory where a Regge trajectory $J = \alpha(0) + \alpha'(0)M^2$ is specified by its intercept $\alpha(0)$ and slope $\alpha'(0)$. It has been argued^{91,92} that $\alpha_J(0) \simeq 0.5$ and $\alpha'_J(0) \simeq 1/3 \alpha'_R(0)$. Regge theory gives exponential rapidity correlations, which in the presence of two sources (at $\pm Y_{\max}$) lead to net baryon rapidity density in central $A + A$ collisions of the form:

$$\frac{dN^{B-\bar{B}}}{dy} = (Z + N)(1 - \alpha_J(0)) \frac{\cosh(1 - \alpha_J(0))y}{\sinh(1 - \alpha_J(0))Y_{\max}}. \quad (52)$$

It is evident from Eq.(52) that the net baryon distribution integrates to $2A$ and in going to peripheral reactions scales as N_{part} . At RHIC energies of $\sqrt{s} = 130(200)$ GeV, corresponding to $Y_{\max} = 4.8(5.4)$, in central reactions $dN^{B-\bar{B}}/dy = d(p-\bar{p})/dy + d(n-\bar{n})/dy + d(\Lambda-\bar{\Lambda})/dy + \dots \simeq 18(13.5)$. The relative contribution of each baryon species can be evaluated from isospin symmetry and strangeness conservation via comparison to midrapidity kaon production.

The high p_T part of the hadron spectra is computed from Eq.(7). Hadronic transport in small-to-moderate p_T is effectively controlled by the slope of the Regge trajectory. This would suggest that the baryon/meson mean inverse slopes in a phenomenological p_T -exponential ($\sim e^{-p_T/T}$) soft particle production model are related as $T_B : T_M \simeq \sqrt{3} : \sqrt{2}$. Soft pion production, however, is largely dominated by resonance decays, where the cumulative effect from the random walk in p_T due to string breaking is destroyed. This leads to the relation $\langle p_T \rangle_\pi : \langle p_T \rangle_K : \langle p_T \rangle_B \simeq 1 : (1 \div \sqrt{2}) : \sqrt{3}$ (220 MeV : 275 MeV : 380 MeV)^{86,87}. One also notes that in the limit of pair production dominated by junction-antijunction loops (which we consider here) the transverse momentum distribution of antibaryons closely resembles that of baryons (with $\langle p_T \rangle_{\bar{B}} = \langle p_T \rangle_B$).

We find an enhanced baryon/meson ratio $R_B(p_T) \geq 1$ that decreases with centrality in a finite p_T window as illustrated in Fig. 19. For $p_T >$

JET QUENCHING AND RADIATIVE ENERGY LOSS IN DENSE NUCLEAR MATTER 33

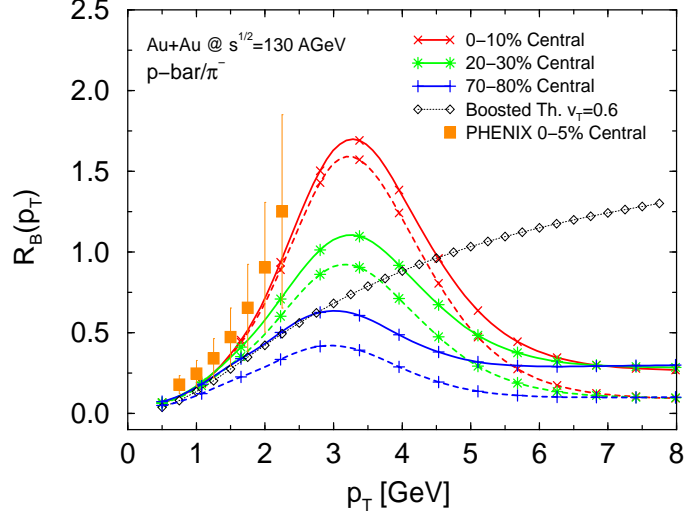


Fig. 19. The \bar{p}/π^- ratio versus p_T for 3 centrality classes at $\sqrt{s_{NN}} = 130$ GeV from Refs.^{86,87}. N_{part} (solid) versus N_{bin} (dashed) geometry is shown. Boosted thermal source computation and ratio of *fits* to PHENIX data are shown for comparison.

5 GeV the ratio is reduced below unity and approaches the perturbative calculation. The centrality dependence of $R_B(p_T)$ is largely driven by the non-Abelian energy loss that suppresses perturbative pion production for $p_T \geq 2$ GeV. It is important to note that an enhanced p/π ratio is also observed in peripheral reactions and is consistent with measurements in $p+p$. In Fig. 20 baryon enhancement is reflected in the different suppression factor $R_{AA}(p_T)$ for neutral pions and inclusive charged hadrons. At high transverse momenta the suppression ratio is expected to be similar and driven by fragmentation of quenched jets. The rate at which this common R_{AA} is approached depends on the fragmentation functions into baryons that are currently poorly constrained or unknown.

2.7. High- p_T Azimuthal Asymmetry

A new way to probe the energy loss ΔE in variable geometries was recently proposed in Ref.^{35,36}. The idea was to exploit the spatial azimuthal asymmetry of non-central nuclear collisions. The dependence of ΔE on the path length $L(\phi)$ naturally results in a pattern of azimuthal asymmetry of high p_T hadrons which can be measured via the differential elliptic flow

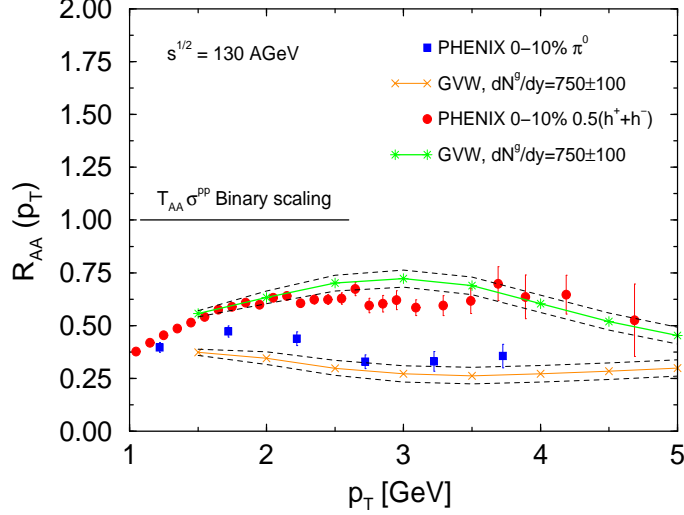


Fig. 20. Suppression of neutral pions and inclusive charged hadrons relative to the binary collision scaled $p + p$ result from Refs.^{86,87}. Central $Au + Au$ at $\sqrt{s_{NN}} = 130$ GeV.

parameter (second Fourier coefficient), $v_2(p_T)$:

$$v_2(p_T) = \frac{\langle p_x^2 \rangle - \langle p_y^2 \rangle}{\langle p_x^2 \rangle + \langle p_y^2 \rangle} = \langle \cos 2\phi \rangle = \frac{\int_0^{2\pi} d\phi \cos 2\phi \frac{dN^h}{dy p_T dp_T d\phi}}{\int_0^{2\pi} d\phi \frac{dN^h}{dy p_T dp_T d\phi}}. \quad (53)$$

In Ref.³⁶ we predicted $v_2(p_T)$ for two models of initial conditions²⁵ (specified by dN^g/dy) which differ by almost an order of magnitude. The longitudinal expansion of the plasma and the corresponding mean energy loss were given by Eqs.(39),(44) with $\alpha = 1$. A novel element of the analysis was the discussion of the interplay between the azimuthally asymmetric soft (hydrodynamic) and hard (quenched jet) components of the final hadron distributions. In non-central $A + B$ reactions the low p_T hadrons are also expected to exhibit azimuthal asymmetry caused by the hydrodynamic flow^{31,94}. We therefore modeled the soft component with the following Ansatz:

$$\frac{dN_s(b)}{dy d^2\mathbf{p}_T} = \frac{dn_s}{dy} \frac{e^{-p_T/T_0}}{2\pi T_0^2} (1 + 2v_{2s}(p_T) \cos(2\phi) + \dots). \quad (54)$$

Here we took $T_0 \approx 0.25$ GeV and incorporate the hydrodynamic elliptic flow predicted in Ref.³¹ and found to grow monotonically with p_T as

$$v_{2s}(p_T) \approx \tanh(p_T/(10 \pm 2 \text{ GeV})). \quad (55)$$

The hydrodynamic elliptic flow was found³¹ to be less sensitive to the initial conditions than the high p_T jet quenching studied in Ref.³⁶.

We showed that the combined pattern of jet quenching in the single inclusive spectra and the differential elliptic flow at high p_T provide complementary tools³⁶ that can determine the effective density of gluons created in the early stages of relativistic heavy ion reactions.

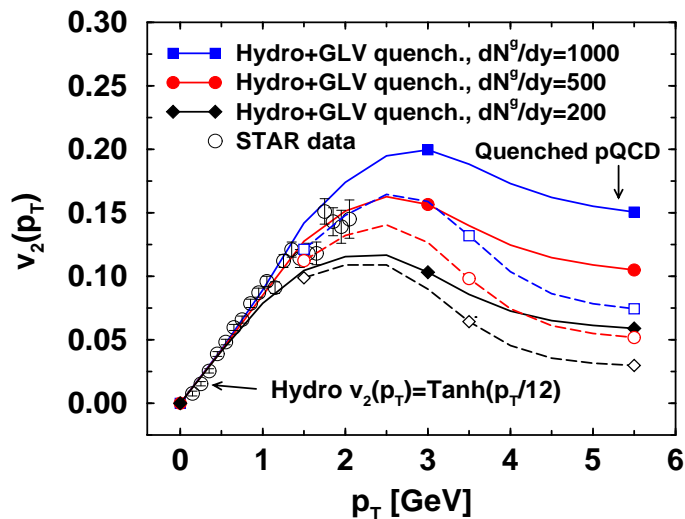


Fig. 21. The interpolation of $v_2(p_T)$ between the soft hydrodynamic^{31,94} and hard pQCD regimes is shown for $b = 7$ fm adapted from Ref.³⁶. Solid (dashed) curves correspond to sharp cylindrical (diffuse Woods-Saxon) geometries.

Fig. 21 shows the predicted pattern of high- p_T anisotropy. Note the difference between sharp cylinder and diffuse Woods-Saxon geometries at $b = 7$ fm approximating roughly 20-30% central events. While the central ($b = 0$) inclusive quenching is insensitive to the density profile, non-central events clearly exhibit large sensitivity to the actual distribution. In particular, the sharp elliptic geometry also simulates one of the possible scenarios of large energy loss and predominant surface emission⁹⁵. We conclude that $v_2(p_T > 2 \text{ GeV}, b)$ provides essential complementary information about the geometry and impact parameter dependence of the initial conditions in $A + A$ reactions and the magnitude of jet quenching. In particular, the rate at which the v_2 coefficient decreases at high p_T is an indicator of the diffuseness of that geometry. Minimum bias STAR data at RHIC⁸ now

confirm the predicted saturation of $v_2(p_T)$. For $p_T \geq 6$ GeV data is still inconclusive due to the large error bars and can still accommodate different scenarios: constant versus slightly decreasing $v_2(p_T)$. High statistics measurements in the future RHIC runs can help to experimentally resolve this question and further test the predicted^{35,36} slow decrease of v_2 at large transverse momenta.

In Refs.^{96,97}, in an independent analysis the GLV radiative energy loss^{52,53} of fast partons was coupled to a dynamically evolving soft hydrodynamic background to obtain a quantitative description of the disappearance of the back-to-back jet correlations⁶.

3. The WW Approach: Parton Energy Loss with Detailed Balance

The above studies of parton energy loss have concentrated on gluon radiation induced by multiple scattering in a medium. Since gluons are bosons, there should also be stimulated gluon emission and absorption by the propagating parton because of the presence of thermal gluons in the hot medium. Such detailed balance is crucial for parton thermalization and should also be important for calculating the energy loss of an energetic parton in a hot medium⁹⁸.

3.1. Final-state Absorption

Let us assume that the hot medium is in thermal equilibrium shortly after the production of the hard parton. One should then take into account of both stimulated emission and thermal absorption in the final state radiation of a jet in a thermal medium with finite temperature T . One has then the probability of gluon radiation with energy ω ,

$$\begin{aligned} \frac{dP^{(0)}}{d\omega} &= \frac{\alpha_s C_F}{2\pi} \int \frac{dz}{z} \int \frac{d\mathbf{k}_\perp^2}{\mathbf{k}_\perp^2} \left[N_g(zE) \delta(\omega + zE) \right. \\ &\quad \left. + (1 + N_g(zE)) \delta(\omega - zE) \theta(1 - z) \right] P\left(\frac{\omega}{E}\right), \end{aligned} \quad (56)$$

where, $N_g(|\mathbf{k}|) = 1/[\exp(|\mathbf{k}|/T) - 1]$ is the thermal gluon distribution. We have define the splitting function $P_{gq}(z) \equiv P(z)/z = [1 + (1 - z)^2]/z$ for $q \rightarrow gq$. The first term is from thermal absorption and the second term from gluon emission with the Bose-Einstein enhancement factor. For $E \gg T$, one can neglect the quantum statistical effect for the leading parton. Note that the vacuum part has a logarithmic infrared divergence while the finite-temperature part has a linear divergence, since $N_g(|\mathbf{k}|) \sim T/|\mathbf{k}|$ as $|\mathbf{k}| \rightarrow 0$.

These infrared divergences will be canceled by the virtual corrections which also contain a zero-temperature and a finite-temperature part. In addition, the virtual corrections are also essential to ensure unitarity and momentum conservation in the QCD evolution of the fragmentation functions. However, they do not contribute to the effective parton energy loss. The remaining collinear divergence in the above spectrum can be absorbed into a renormalized fragmentation function that follows the QCD evolution equations.

Subtracting the gluon radiation spectrum in the vacuum, one then obtains the energy loss due to final-state absorption and stimulated emission,

$$\begin{aligned} \Delta E_{abs}^{(0)} &= \int d\omega \omega \left(\frac{dP^{(0)}}{d\omega} - \frac{dP^{(0)}}{d\omega} \Big|_{T=0} \right) \\ &= \frac{\alpha_s C_F}{2\pi} E \int dz \int_{\mu^2}^{k_{\perp}^{max}} \frac{d\mathbf{k}_{\perp}^2}{\mathbf{k}_{\perp}^2} \left[-P(-z)N_g(zE) \right. \\ &\quad \left. + P(z)N_g(zE)\theta(1-z) \right]. \end{aligned} \quad (57)$$

Even though the stimulated emission cancels part of the contribution from absorption, the net medium effect without rescattering is still dominated by the final-state thermal absorption, resulting in a net energy gain, *i.e.* a *negative* energy loss. For asymptotically large parton energy, $E \gg T$, one can complete the above integration approximately and have,

$$\frac{\Delta E_{abs}^{(0)}}{E} \approx -\frac{\pi\alpha_s C_F}{3} \frac{T^2}{E^2} \left[\ln \frac{4ET}{\mu^2} + 2 - \gamma_E + \frac{6\zeta'(2)}{\pi^2} \right], \quad (58)$$

where, $\gamma_E \approx 0.5772$ and $\zeta'(2) \approx -0.9376$. The quadratic temperature dependence of the leading contribution is a direct consequence of the partial cancellation between stimulated emission and thermal absorption, each having a leading contribution linear in T .

3.2. Induced Absorption

As in the case of final-state absorption, one can also include stimulated emission and thermal absorption when calculating the induced radiation

probability at the first order in opacity,

$$\begin{aligned}
\frac{dP^{(1)}}{d\omega} &= \frac{C_2}{8\pi d_A d_R} \int \frac{dz}{z} \int \frac{d^2 \mathbf{k}_\perp}{(2\pi)^2} \int \frac{d^2 \mathbf{q}_\perp}{(2\pi)^2} v^2(\mathbf{q}_\perp) P\left(\frac{\omega}{E}\right) \\
&\times \frac{N}{A_\perp} \left\langle \text{Tr} \left[|R^{(S)}|^2 + 2\text{Re} \left(R^{(0)\dagger} R^{(D)} \right) \right] \right\rangle \\
&\times \left[(1 + N_g(zE)) \delta(\omega - zE) \theta(1 - z) + N_g(zE) \delta(\omega + zE) \right] \\
&= \frac{\alpha_s C_2 C_F C_A}{d_A \pi} \int \frac{dz}{z} \int \frac{d\mathbf{k}_\perp^2}{\mathbf{k}_\perp^2} \int \frac{d^2 \mathbf{q}_\perp}{(2\pi)^2} v^2(\mathbf{q}_\perp) P\left(\frac{\omega}{E}\right) \\
&\times \frac{\mathbf{k}_\perp \cdot \mathbf{q}_\perp}{(\mathbf{k}_\perp - \mathbf{q}_\perp)^2} \frac{N}{A_\perp} \left\langle \text{Re}(1 - e^{i\omega_1 y_{10}}) \right\rangle \left[N_g(zE) \delta(\omega + zE) \right. \\
&\left. + (1 + N_g(zE)) \delta(\omega - zE) \theta(1 - z) \right]. \tag{59}
\end{aligned}$$

The factor $1 - \exp(i\omega_1 y_{10})$ reflects the destructive interference arising from the non-Abelian LPM effect. The target distribution is assumed to be an exponential form $\rho(y) = 2 \exp(-2y/L)/L$.

As in the final-state absorption, the contribution from thermal absorption associated with rescattering is larger than that of stimulated emission, resulting in a net energy gain. However, the zero-temperature contribution corresponds to the radiation induced by rescattering which will lead to an effective energy loss by the leading parton. This is the energy loss obtained the previous sections and we denote this part as $\Delta E_{rad}^{(1)}$. The remainder or temperature-dependent part of energy loss induced by rescattering at the first order in opacity is then defined as

$$\Delta E_{abs}^{(1)} = \int d\omega \omega \left(\frac{dP^{(1)}}{d\omega} - \frac{dP^{(1)}}{d\omega} \Big|_{T=0} \right), \tag{60}$$

which mainly comes from thermal absorption with partial cancellation by stimulated emission in the medium. According to Eq.(59),

$$\begin{aligned}
\Delta E_{rad}^{(1)} &= \frac{\alpha_s C_F}{\pi} \frac{L}{\lambda_g} E \int dz \int \frac{d\mathbf{k}_\perp^2}{\mathbf{k}_\perp^2} \int d^2 \mathbf{q}_\perp |\bar{v}(\mathbf{q}_\perp)|^2 \frac{\mathbf{k}_\perp \cdot \mathbf{q}_\perp}{(\mathbf{k}_\perp - \mathbf{q}_\perp)^2} \\
&\times P(z) \left\langle \text{Re}(1 - e^{i\omega_1 y_{10}}) \right\rangle \theta(1 - z); \tag{61}
\end{aligned}$$

$$\begin{aligned}
\Delta E_{abs}^{(1)} &= \frac{\alpha_s C_F}{\pi} \frac{L}{\lambda_g} E \int dz \int \frac{d\mathbf{k}_\perp^2}{\mathbf{k}_\perp^2} \int d^2 \mathbf{q}_\perp |\bar{v}(\mathbf{q}_\perp)|^2 \frac{\mathbf{k}_\perp \cdot \mathbf{q}_\perp}{(\mathbf{k}_\perp - \mathbf{q}_\perp)^2} \\
&\times N_g(zE) \left[P(z) \left\langle \text{Re}(1 - e^{i\omega_1 y_{10}}) \right\rangle \theta(1 - z) \right. \\
&\left. - P(-z) \left\langle \text{Re}(1 - e^{i\omega_1 y_{10}}) \right\rangle \right], \tag{62}
\end{aligned}$$

In the limit $q_{\perp max} \rightarrow \infty$, the angular integral can be carried out by partial integration. These contributions to the energy loss become

$$\Delta E_{rad}^{(1)} \approx \frac{\alpha_s C_F}{2\pi} \frac{L}{\lambda_g} E \int dz P(z) h(\gamma) \theta(1-z); \quad (63)$$

$$\Delta E_{abs}^{(1)} \approx \frac{\alpha_s C_F}{2\pi} \frac{L}{\lambda_g} E \int dz N_g(zE) h(\gamma) [P(z)\theta(1-z) - P(-z)], \quad (64)$$

where, $\gamma = \mu^2 L / (4zE)$ and

$$h(\gamma) = \begin{cases} \frac{2\gamma}{\sqrt{1-4\gamma^2}} \left[\frac{\pi}{2} - \arcsin(2\gamma) \right], & \gamma < 1/2 \\ \frac{2\gamma}{\sqrt{4\gamma^2-1}} \ln[2\gamma + \sqrt{4\gamma^2-1}], & \gamma > 1/2. \end{cases} \quad (65)$$

One can approximate $h(\gamma)$ with $\pi\gamma + (11/4 - 2\pi)\gamma^2 + (5/2)\gamma^3$ for $\gamma < 1/2$ and $\ln(4\gamma) + 0.1/\gamma + 0.028/\gamma^2$ for $\gamma > 1/2$. In the limit of $EL \gg 1$ and $E \gg \mu$, One can then get the approximate asymptotic behavior of the energy loss,

$$\frac{\Delta E_{rad}^{(1)}}{E} \approx \frac{\alpha_s C_F \mu^2 L^2}{4\lambda_g E} \left[\ln \frac{2E}{\mu^2 L} - 0.048 \right]; \quad (66)$$

$$\frac{\Delta E_{abs}^{(1)}}{E} \approx -\frac{\pi\alpha_s C_F}{3} \frac{LT^2}{\lambda_g E^2} \left[\ln \frac{\mu^2 L}{T} - 1 + \gamma_E - \frac{6\zeta'(2)}{\pi^2} \right]. \quad (67)$$

Again, the thermal absorption results in an energy gain (or negative energy loss). This result is accurate through the order of $1/E$. In Eq.(67), we have assumed $\mu^2 L/T \gg 1$ and kept only the first two leading terms. In this limit, the average formation time for stimulated emission or thermal absorption is much smaller than the total propagation length. Therefore, the energy gain, $\Delta E_{abs}^{(1)}$, by thermal absorption (with partial cancellation by the stimulated emission) is linear in L , as compared to the quadratic dependence in the zero-temperature case. However, the logarithmic dependence on $\mu^2 L/T$, as compared to the factor $\ln(4ET/\mu^2)$ in Eq.(58) for no rescattering, is still a consequence of the LPM interference in medium. A quadratic L -dependence of $\Delta E_{abs}^{(1)}$ will arise when $\mu^2 L/T \ll 1$.

To evaluate the effect of thermal absorption numerically, we assume the Debye screening mass to be $\mu^2 = 4\pi\alpha_s T^2$ from the perturbative QCD at finite temperature⁹⁹. The mean-free-path for a gluon λ_g in the GW model is⁷²,

$$\lambda_g^{-1} = \langle \sigma_{qg}\rho_q \rangle + \langle \sigma_{gg}\rho_g \rangle \approx \frac{2\pi\alpha_s^2}{\mu^2} 9 \times 7\zeta(3) \frac{T^3}{\pi^2}, \quad (68)$$

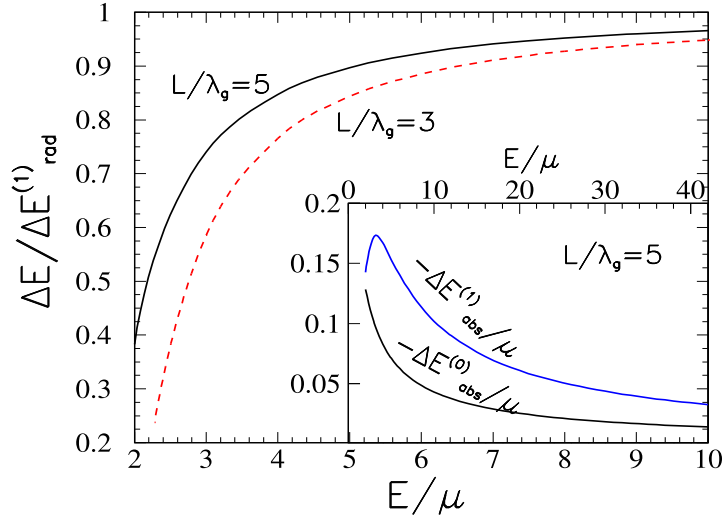


Fig. 22. The ratio of effective parton energy loss with ($\Delta E = \Delta E_{abs}^{(0)} + \Delta E_{abs}^{(1)} + \Delta E_{rad}^{(1)}$) and without ($\Delta E_{rad}^{(1)}$) absorption as a function of E/μ . Inset box: energy gain via absorption with ($\Delta E_{abs}^{(1)}$) and without ($\Delta E_{abs}^{(0)}$) rescattering.

where $\zeta(3) \approx 1.202$. With fixed values of L/λ_g and α_s , $\Delta E/\mu$ should be a function of E/μ only. Shown in Fig. 22 are ratios of the calculated radiative energy loss with and without stimulated emission and thermal absorption as functions of E/μ for $L/\lambda_g = 3, 5$ and $\alpha_s = 0.3$. Shown in the inset box are the energy gain via gluon absorption with ($\Delta E_{abs}^{(1)}$) and without ($\Delta E_{abs}^{(0)}$) rescattering. For partons with very high energy the effect of the gluon absorption is small and can be neglected. However, the thermal absorption reduces the effective parton energy loss by about 30-10% for intermediate values of parton energy. This will increase the energy dependence of the effective parton energy loss in the intermediate energy region. The observed flat or slightly p_T dependence of the hadron spectra suppression indicates a strong energy dependence of the parton energy loss. This might indicate the effect of the thermal absorption, in particular in the intermediate p_T region.

4. The WOGZ Approach: Parton Energy Loss and Modified Fragmentation Functions in Nuclei

So far we have reviewed the parton energy loss of an energetic parton induced by multiple scattering in a hot QCD medium. The effective parton energy loss is shown to be proportional to the gluon density. Therefore measurements of the parton energy loss will enable one to extract the initial gluon density of the produced hot medium within our assumed screened potential model for multiple parton scattering in a dense gluonic medium. Such an exercise will be more robust if one can also measure the parton energy loss and the gluon density inside a cold nuclear medium. For this purpose, one has to rely on other complementary experimental measurements such as parton energy loss in deeply inelastic scattering (DIS) off nuclear targets. One can then study parton energy loss and extract the initial gluon density in high-energy heavy-ion collisions relative to that in a cold nucleus⁷¹.

Extending the screened potential model of multiple parton scattering to a cold nuclear medium is somewhat problematic because it applies mainly to a medium where colors are screened but not confined. In this section we will study parton multiple scattering inside a nucleus where colors are confined to the size of a nucleon within generalized factorization theory of pQCD. In this case, parton propagation will be different from that in a partonic medium and one should expect the parton energy loss to be related to the nucleon size or confinement scale which, as we shall show, can be related to the gluon density inside a cold nucleus. In addition, one can calculate directly the modification of the fragmentation functions due to multiple scattering and induced gluon bremsstrahlung. This section reviews developments published in Refs.^{69,70,101,104}, which are referred to here as WOGZ and are applied in Ref.⁷¹ to cold and hot nuclei.

In contrast to the situation in QED, the energy loss of a parton cannot be directly measured because partons are not the final experimentally observed particles. The total energy of a jet, traditionally defined as a cluster of hadrons in the phase space, will not change much due to medium induced radiation, because a jet so defined contains particles both from the leading parton and from the radiated gluons. This is particularly the case if multiple scattering and induced radiation do not *dramatically* change the energy profile of the jet in phase-space. It is also virtually impossible to determine the jet energy event by event because of the large background and its fluctuation in heavy-ion collisions. One then has to resort to parti-

cle distributions within a jet and study the effect of parton energy loss by measuring the modification of the fragmentation function of the produced parton, $D_{a \rightarrow h}(z, \mu^2)$, where z is the fractional energy of the parton a carried by the produced particles h .

Since the produced quark in DIS is far off-shell, the final-state radiation leads to the scale dependence of the fragmentation functions as given by Dokshitzer-Gribov-Lipatov-Altarelli-Parisi (DGLAP)¹⁰⁰ QCD evolution equations. When a parton is produced in a medium, it will suffer multiple scattering and induced radiation that will give rise to an additional term in the DGLAP evolution equations. This then leads to the medium modification of the DGLAP evolution of the parton fragmentation functions. As a consequence, the modified fragmentation functions become softer. This can be directly translated into the energy loss of the leading quark.

4.1. Generalized Factorization

To study parton energy loss in eA DIS, we consider the semi-inclusive processes, $e(L_1) + A(p) \rightarrow e(L_2) + h(\ell_h) + X$, where L_1 and L_2 are the four-momenta of the incoming and the outgoing leptons, and ℓ_h is the observed hadron momentum. The differential cross section for the semi-inclusive process can be expressed as

$$E_{L_2} E_{\ell_h} \frac{d\sigma_{\text{DIS}}^h}{d^3 L_2 d^3 \ell_h} = \frac{\alpha_{\text{EM}}^2}{2\pi s} \frac{1}{Q^4} L_{\mu\nu} E_{\ell_h} \frac{dW^{\mu\nu}}{d^3 \ell_h}, \quad (69)$$

where $p = [p^+, 0, \mathbf{0}_\perp]$ is the momentum per nucleon in the nucleus, $q = L_2 - L_1 = [-Q^2/2q^-, q^-, \mathbf{0}_\perp]$ the momentum transfer, $s = (p + L_1)^2$ and α_{EM} is the electromagnetic (EM) coupling constant. The leptonic tensor is given by $L_{\mu\nu} = 1/2 \text{Tr}(\gamma \cdot L_1 \gamma_\mu \gamma \cdot L_2 \gamma_\nu)$ while the semi-inclusive hadronic tensor is defined as,

$$E_{\ell_h} \frac{dW_{\mu\nu}}{d^3 \ell_h} = \frac{1}{2} \sum_X \langle A | J_\mu(0) | X, h \rangle \langle X, h | J_\nu(0) | A \rangle \\ \times 2\pi \delta^4(q + p - p_X - \ell_h) \quad (70)$$

where \sum_X runs over all possible final states and $J_\mu = \sum_q e_q \bar{\psi}_q \gamma_\mu \psi_q$ is the hadronic EM current.

In the parton model with the collinear factorization approximation, the leading-twist contribution to the semi-inclusive cross section can be factorized into a product of parton distributions, parton fragmentation functions

and the partonic cross section. Including all leading log radiative corrections, the lowest order contribution ($\mathcal{O}(\alpha_s^0)$) from a single hard $\gamma^* + q$ scattering can be written as

$$\frac{dW_{\mu\nu}^S}{dz_h} = \sum_q e_q^2 \int dx f_q^A(x, \mu_I^2) H_{\mu\nu}^{(0)}(x, p, q) D_{q \rightarrow h}(z_h, \mu^2); \quad (71)$$

$$H_{\mu\nu}^{(0)}(x, p, q) = \frac{1}{2} \text{Tr}(\gamma \cdot p \gamma_\mu \gamma \cdot (q + xp) \gamma_\nu) \frac{2\pi}{2p \cdot q} \delta(x - x_B), \quad (72)$$

where the momentum fraction carried by the hadron is defined as $z_h = \ell_h^-/q^-$ and $x_B = Q^2/2p^+q^-$ is the Bjorken variable. μ_I^2 and μ^2 are the factorization scales for the initial quark distributions $f_q^A(x, \mu_I^2)$ in a nucleus and the fragmentation functions $D_{q \rightarrow h}(z_h, \mu^2)$, respectively. Considering the leading logarithm approximation of the radiative correction to the fragmentation process as shown in Fig. 23, the renormalized quark fragmentation function $D_{q \rightarrow h}(z_h, \mu^2)$ satisfies the DGLAP¹⁰⁰ QCD evolution equations,

$$\begin{aligned} \frac{\partial D_{q \rightarrow h}(z_h, \mu^2)}{\partial \ln \mu^2} &= \frac{\alpha_s(\mu^2)}{2\pi} \int_{z_h}^1 \frac{dz}{z} [\gamma_{q \rightarrow qq}(z) D_{q \rightarrow h}(z_h/z, \mu^2) \\ &+ \gamma_{q \rightarrow gq}(z) D_{g \rightarrow h}(z_h/z, \mu^2)] , \end{aligned} \quad (73)$$

where

$$\gamma_{q \rightarrow qq}(z) = C_F \left[\frac{1+z^2}{(1-z)_+} + \frac{3}{2} \delta(1-z) \right], \quad (74)$$

$$\gamma_{q \rightarrow gq}(z) = \gamma_{q \rightarrow qg}(1-z) \quad (75)$$

are the splitting functions. The ‘+’ function is defined as

$$\int_0^1 dz \frac{F(z)}{(1-z)_+} \equiv \int_0^1 dz \frac{F(z) - F(1)}{1-z} \quad (76)$$

with $F(z)$ being any function which is sufficiently smooth at $z = 1$.

In a nuclear medium, the propagating quark in DIS will experience additional scatterings with other partons from the nucleus. The rescatterings may induce additional gluon radiation and cause the leading quark to lose energy. Such induced gluon radiations will effectively give rise to additional terms in the evolution equation leading to the modification of the fragmentation functions in a medium. These are the so-called higher-twist corrections since they involve higher-twist parton matrix elements and are power-suppressed. We will consider those contributions that involve two-parton correlations from two different nucleons inside the nucleus. They

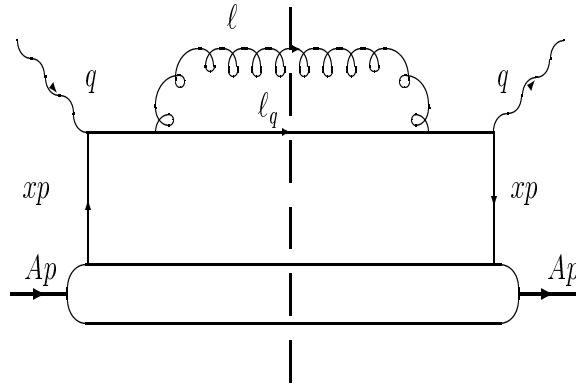


Fig. 23. The hard partonic part of the first order radiative correction to the fragmentation process.

are proportional to the size of the nucleus¹⁰¹ and thus are enhanced by a nuclear factor $A^{1/3}$ as compared to two-parton correlations in a nucleon. As in previous studies^{69,70}, we will neglect those contributions that are not enhanced by the nuclear medium.

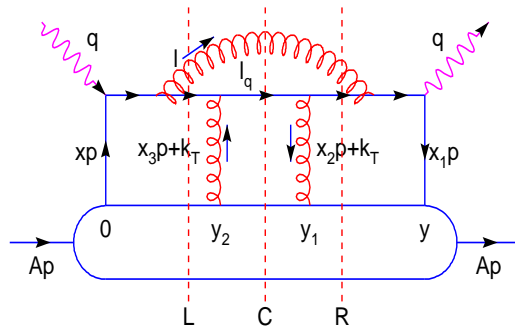


Fig. 24. A typical diagram for quark-gluon re-scattering processes with three possible cuts, central(C), left(L) and right(R).

We will employ the generalized factorization of multiple scattering processes¹⁰². In this approximation, the double scattering contribution to radiative correction from processes like the one illustrated in Fig. 24 can

be written in the following form,

$$\begin{aligned} \frac{dW_{\mu\nu}^D}{dz_h} &= \sum_q \int_{z_h}^1 \frac{dz}{z} D_{q \rightarrow h}(z_h/z) \int \frac{dy^-}{2\pi} dy_1^- dy_2^- \frac{d^2 y_T}{(2\pi)^2} d^2 k_T \\ &\times e^{-i\mathbf{k}_T \cdot \mathbf{y}_T} \overline{H}_{\mu\nu}^D(y^-, y_1^-, y_2^-, k_T, p, q, z); \\ &\times \frac{1}{2} \langle A | \bar{\psi}_q(0) \gamma^+ A^+(y_2^-, 0_T) A^+(y_1^-, y_T) \psi_q(y^-) | A \rangle . \end{aligned} \quad (77)$$

Here $\overline{H}_{\mu\nu}^D(y^-, y_1^-, y_2^-, k_T, p, q, z)$ is the Fourier transform of the partonic hard part $\tilde{H}_{\mu\nu}(x, x_1, x_2, k_T, p, q, z)$ in momentum space,

$$\begin{aligned} \overline{H}_{\mu\nu}^D(y^-, y_1^-, y_2^-, k_T, p, q, z) &= \int dx \frac{dx_1}{2\pi} \frac{dx_2}{2\pi} e^{ix_1 p^+ y^- + ix_2 p^+ y_1^-} \\ &\times e^{i(x-x_1-x_2)p^+ y_2^-} \tilde{H}_{\mu\nu}^D(x, x_1, x_2, k_T, p, q, z) , \end{aligned} \quad (78)$$

where k_T is the relative transverse momentum carried by the second parton in the double scattering. Values of the momentum fractions x, x_1 and x_2 are fixed by δ -functions and poles in the partonic hard part. They normally depend on k_T .

In order to pick up the next-leading-twist contribution, we expand the partonic hard part around $k_T = 0$,

$$\begin{aligned} \overline{H}_{\mu\nu}^D(y^-, y_1^-, y_2^-, k_T, p, q, z) &= \overline{H}_{\mu\nu}^D(y^-, y_1^-, y_2^-, k_T = 0, p, q, z) \\ &+ \left. \frac{\partial \overline{H}_{\mu\nu}^D}{\partial k_T^\alpha} \right|_{k_T=0} k_T^\alpha + \frac{1}{2} \left. \frac{\partial^2 \overline{H}_{\mu\nu}^D}{\partial k_T^\alpha \partial k_T^\beta} \right|_{k_T=0} k_T^\alpha k_T^\beta + \dots . \end{aligned} \quad (79)$$

This is known as the collinear expansion¹⁰³. On the right-hand-side of Eq.(79), the first term gives the eikonal contribution to the leading-twist results. It does not correspond to the physical double scattering, but simply makes the matrix element in a single scattering gauge invariant. The second term for unpolarized initial and final states vanishes after being integrated over k_T . The third term will give a finite contribution to the double scattering process. Substituting Eq.(79) into Eq.(77), integrating over $d^2 k_T$ and $d^2 y_T$, we obtain

$$\begin{aligned} \frac{dW_{\mu\nu}^D}{dz_h} &= \sum_q \int_{z_h}^1 \frac{dz}{z} D_{q \rightarrow h}(z_h/z) \int \frac{dy^-}{2\pi} dy_1^- dy_2^- \\ &\times \frac{1}{2} \langle A | \bar{\psi}_q(0) \gamma^+ F_{\sigma^+}(y_2^-) F^{+\sigma}(y_1^-) \psi_q(y^-) | A \rangle \\ &\times \left(-\frac{1}{2} g^{\alpha\beta} \right) \left[\frac{1}{2} \frac{\partial^2}{\partial k_T^\alpha \partial k_T^\beta} \overline{H}_{\mu\nu}^D(y^-, y_1^-, y_2^-, k_T, p, q, z) \right]_{k_T=0} , \end{aligned} \quad (80)$$

where $k_T^\alpha A^+ k_T^\beta A^+$ are converted into field strength $F^{\alpha+} F^{\beta+}$ by partial integrations.

4.2. Double Parton Scattering

There are all together 23 cut-diagrams that contribute to the leading twist-four corrections to the quark fragmentation function in eA DIS. For simplification of the calculation, one can use the helicity amplitude approximation by Guo and Wang^{69,70} in the limit of soft gluon radiation. Such an approximation enables one to simplify the calculation of the radiation amplitudes. However, a complete calculation of the all cut-diagrams were recently done by Zhang and Wang¹⁰⁴. Before we list the results, we first consider the contribution from Fig. 24 in detail.

Using the conventional Feynman rule, one can write down the hard partonic part of the central cut-diagram of Fig. 24^{69,70},

$$\begin{aligned} \overline{H}_{C\mu\nu}^D(y^-, y_1^-, y_2^-, k_T, p, q, z) &= \int dx \frac{dx_1}{2\pi} \frac{dx_2}{2\pi} e^{ix_1 p^+ y^- + ix_2 p^+ y_1^-} \\ &\times e^{i(x-x_1-x_2)p^+ y_2^-} \int \frac{d^4\ell}{(2\pi)^4} \frac{1}{2} \text{Tr} \left[p \cdot \gamma \gamma_\mu p^\sigma p^\rho \widehat{H}_{\sigma\rho} \gamma_\nu \right] \\ &\times 2\pi \delta_+(\ell^2) \delta\left(1 - z - \frac{\ell^-}{q^-}\right). \end{aligned} \quad (81)$$

$$\begin{aligned} \widehat{H}_{\sigma\rho} &= \frac{C_F}{2N_c} g^4 \frac{\gamma \cdot (q + x_1 p)}{(q + x_1 p)^2 - i\epsilon} \gamma_\alpha \frac{\gamma \cdot (q + x_1 p - \ell)}{(q + x_1 p - \ell)^2 - i\epsilon} \gamma_\sigma \gamma \cdot \ell_q \gamma_\rho \\ &\times \varepsilon^{\alpha\beta}(\ell) \frac{\gamma \cdot (q + xp - \ell)}{(q + xp - \ell)^2 + i\epsilon} \gamma_\beta \frac{\gamma \cdot (q + xp)}{(q + xp)^2 + i\epsilon} 2\pi \delta_+(\ell_q^2), \end{aligned} \quad (82)$$

where $\varepsilon^{\alpha\beta}(\ell)$ is the polarization tensor of a gluon propagator in an axial gauge, $n \cdot A = 0$ with $n = [1, 0^-, \mathbf{0}_\perp]$, and $\ell, \ell_q = q + (x_1 + x_2)p + k_T - \ell$ are the 4-momenta carried by the gluon and the final quark, respectively. $z = \ell_q^-/q^-$ is the fraction of longitudinal momentum (the large minus component) carried by the final quark.

To simplify the calculation, we apply the collinear approximation to complete the trace of the product of γ -matrices,

$$p^\sigma \widehat{H}_{\sigma\rho} p^\rho \approx \gamma \cdot \ell_q \frac{1}{4\ell_q^-} \text{Tr} \left[\gamma^- p^\sigma \widehat{H}_{\sigma\rho} p^\rho \right]. \quad (83)$$

After carrying out momentum integrations in x, x_1, x_2 and ℓ^\pm with the help of contour integration and δ -functions, the partonic hard part can

JET QUENCHING AND RADIATIVE ENERGY LOSS IN DENSE NUCLEAR MATTER 47

be factorized into the product of γ -quark scattering matrix $H_{\mu\nu}^{(0)}(x, p, q)$ [Eq.(72)] and the quark-gluon rescattering part \overline{H}^D ,

$$\overline{H}_{\mu\nu}^D(y^-, y_1^-, y_2^-, k_T, p, q, z) = \int dx H_{\mu\nu}^{(0)}(x, p, q) \times \overline{H}^D(y^-, y_1^-, y_2^-, k_T, x, p, q, z). \quad (84)$$

Contributions from all the diagrams have this factorized form. Therefore, we will only list the rescattering part \overline{H}^D for different diagrams in the following. For the central-cut diagram in Fig. 24 it reads^{69,70},

$$\overline{H}_{C(\text{Fig.24})}^D(y^-, y_1^-, y_2^-, k_T, x, p, q, z) = \int \frac{d\ell_T^2}{\ell_T^2} \frac{\alpha_s}{2\pi} C_F \frac{1+z^2}{1-z} \times \frac{2\pi\alpha_s}{N_c} \overline{I}_{C(\text{Fig.24})}(y^-, y_1^-, y_2^-, \ell_T, k_T, x, p, q, z), \quad (85)$$

$$\overline{I}_{C(\text{Fig.24})}(y^-, y_1^-, y_2^-, \ell_T, k_T, x, p, q, z) = e^{i(x+x_L)p^+y^- + ix_D p^+(y_1^- - y_2^-)} \theta(-y_2^-) \times \theta(y^- - y_1^-) (1 - e^{-ix_L p^+ y_2^-}) (1 - e^{-ix_L p^+(y^- - y_1^-)}). \quad (86)$$

Here, the fractional momentum is defined as

$$x_L = \frac{\ell_T^2}{2p^+ q^- z(1-z)}, \quad x_D = \frac{k_T^2 - 2\mathbf{k}_T \cdot \ell_T}{2p^+ q^- z}, \quad (87)$$

and $x = x_B = Q^2/2p^+ q^-$ is the Bjorken variable.

The above contribution resembles the cross section of a dipole scattering and contains essentially four terms. The first diagonal term corresponds to the so-called hard-soft process where the gluon radiation is induced by the hard scattering between the virtual photon and an initial quark with momentum fraction x . The quark is knocked off-shell by the virtual photon and becomes on-shell again after radiating a gluon. Afterwards the on-shell quark (or the radiated gluon) will have a secondary scattering with another soft gluon from the nucleus. The second diagonal term is due to the double hard process where the quark is on-shell after the first hard scattering with the virtual photon. The gluon radiation is then induced by the scattering of the quark with another gluon that carries finite momentum fraction $x_L + x_D$. The other two off-diagonal terms are interferences between hard-soft and double hard processes. In the limit of collinear radiation ($x_L \rightarrow 0$) or when the formation time of the gluon radiation, $\tau_f \equiv 1/x_L p^+$, is much larger than the nuclear size, the two processes have destructive interference, leading to the LPM interference effect.

One can similarly obtain the rescattering part \overline{H}^D of other central-cut diagrams (a-d) in Fig. 25:

$$\begin{aligned}\overline{H}_{C(a)}^D(y^-, y_1^-, y_2^-, k_T, x, p, q, z) &= \int \frac{d\ell_T^2}{(\ell_{\mathbf{T}} - \mathbf{k}_{\mathbf{T}})^2} \frac{\alpha_s}{2\pi} C_A \frac{1+z^2}{1-z} \\ &\quad \times \frac{2\pi\alpha_s}{N_c} \overline{I}_{C(a)}(y^-, y_1^-, y_2^-, \ell_T, k_T, x, p, q, z), \\ \overline{I}_{C(a)}(y^-, y_1^-, y_2^-, \ell_T, k_T, x, p, q, z) &= e^{i(x+x_L)p^+y^- + ix_D p^+(y_1^- - y_2^-)} \theta(-y_2^-) \\ &\quad \times \theta(y^- - y_1^-) [e^{ix_D p^+ y_2^- / (1-z)} - e^{-ix_L p^+ y_2^-}] \\ &\quad \times [e^{ix_D p^+(y^- - y_1^-) / (1-z)} - e^{-ix_L p^+(y^- - y_1^-)}],\end{aligned}\quad (88)$$

$$\begin{aligned}\overline{H}_{C(b)}^D(y^-, y_1^-, y_2^-, k_T, x, p, q, z) &= \int \frac{d\ell_T^2}{(\ell_{\mathbf{T}} - (1-z)\mathbf{k}_{\mathbf{T}})^2} \frac{\alpha_s}{2\pi} C_F \frac{1+z^2}{1-z} \\ &\quad \times \frac{2\pi\alpha_s}{N_c} \overline{I}_{C(b)}(y^-, y_1^-, y_2^-, \ell_T, k_T, x, p, q, z), \\ \overline{I}_{C(b)}(y^-, y_1^-, y_2^-, \ell_T, k_T, x, p, q, z) &= e^{i(x+x_L)p^+y^- + ix_D p^+(y_1^- - y_2^-)} \theta(-y_2^-) \\ &\quad \times \theta(y^- - y_1^-) e^{-ix_L p^+(y^- - y_1^-)} e^{-ix_L p^+ y_2^-},\end{aligned}\quad (89)$$

$$\begin{aligned}\overline{H}_{C(c)}^D(y^-, y_1^-, y_2^-, k_T, x, p, q, z) &= \int d\ell_T^2 \frac{(\ell_{\mathbf{T}} - \mathbf{k}_{\mathbf{T}}) \cdot (\ell_{\mathbf{T}} - (1-z)\mathbf{k}_{\mathbf{T}})}{(\ell_{\mathbf{T}} - \mathbf{k}_{\mathbf{T}})^2 (\ell_{\mathbf{T}} - (1-z)\mathbf{k}_{\mathbf{T}})^2} \\ &\quad \times \frac{\alpha_s}{2\pi} \frac{C_A}{2} \frac{1+z^2}{1-z} \frac{2\pi\alpha_s}{N_c} \overline{I}_{C(c)}(y^-, y_1^-, y_2^-, \ell_T, k_T, x, p, q, z), \\ \overline{I}_{C(c)}(y^-, y_1^-, y_2^-, \ell_T, k_T, x, p, q, z) &= e^{i(x+x_L)p^+y^- + ix_D p^+(y_1^- - y_2^-)} \theta(-y_2^-) \\ &\quad \times \theta(y^- - y_1^-) e^{-ix_L p^+ y_2^-} \\ &\quad \times [e^{ix_D p^+(y^- - y_1^-) / (1-z)} - e^{-ix_L p^+(y^- - y_1^-)}],\end{aligned}\quad (90)$$

$$\begin{aligned}\overline{H}_{C(d)}^D(y^-, y_1^-, y_2^-, k_T, x, p, q, z) &= \int d\ell_T^2 \frac{(\ell_{\mathbf{T}} - \mathbf{k}_{\mathbf{T}}) \cdot (\ell_{\mathbf{T}} - (1-z)\mathbf{k}_{\mathbf{T}})}{(\ell_{\mathbf{T}} - \mathbf{k}_{\mathbf{T}})^2 (\ell_{\mathbf{T}} - (1-z)\mathbf{k}_{\mathbf{T}})^2} \\ &\quad \times \frac{\alpha_s}{2\pi} \frac{C_A}{2} \frac{1+z^2}{1-z} \frac{2\pi\alpha_s}{N_c} \overline{I}_{C(d)}(y^-, y_1^-, y_2^-, \ell_T, k_T, x, p, q, z), \\ \overline{I}_{C(d)}(y^-, y_1^-, y_2^-, \ell_T, k_T, x, p, q, z) &= e^{i(x+x_L)p^+y^- + ix_D p^+(y_1^- - y_2^-)} \theta(-y_2^-) \\ &\quad \times \theta(y^- - y_1^-) e^{-ix_L p^+(y^- - y_1^-)} \\ &\quad \times [e^{ix_D p^+ y_2^- / (1-z)} - e^{-ix_L p^+ y_2^-}].\end{aligned}\quad (91)$$

To complete the calculation we also have to consider the asymmetrical-cut diagrams (left-cut and right-cut) that represent interferences between

single and triple scatterings. They can be obtained with similar procedures. We refer readers to Ref.¹⁰⁴ for a list of the the rescattering part \overline{H}^D of all those asymmetrical-cut diagrams.

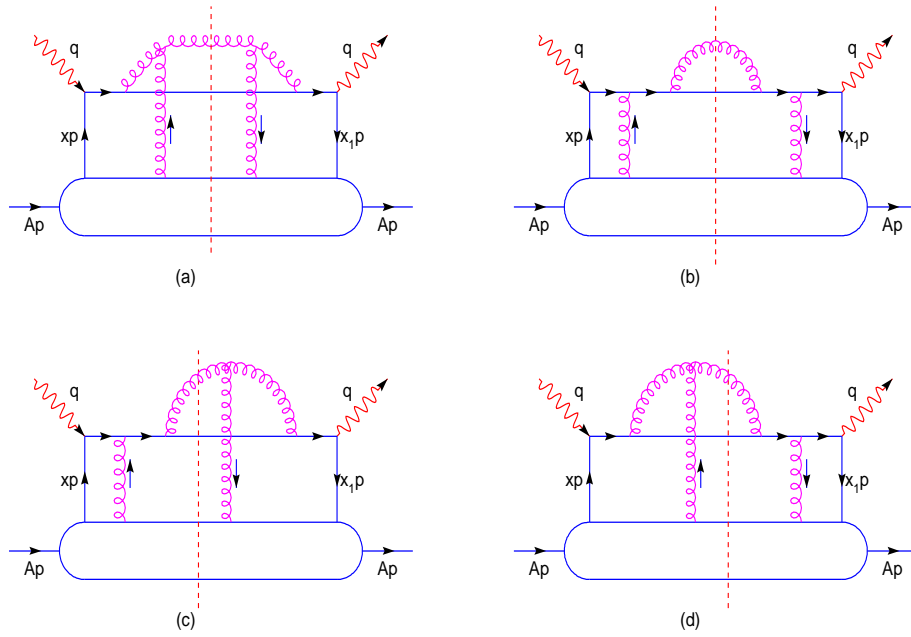


Fig. 25. Four central-cut diagrams that contribute to the final results.

To obtain the double scattering contribution to the semi-inclusive processes of hadron production in Eq.(80), one will then have to calculate the second derivatives of the rescattering part \overline{H}^D . After a closer examination of these rescattering parts, one can find that all contributions from the asymmetrical-cut diagrams have the form

$$\overline{H}_{asym}^D = \frac{\ell_{\mathbf{T}} \cdot (\ell_{\mathbf{T}} - f(z)\mathbf{k}_{\mathbf{T}})}{\ell_{\mathbf{T}}^2 (\ell_{\mathbf{T}} - f(z)\mathbf{k}_{\mathbf{T}})^2} e^{iXp^+Y^-}, \quad (92)$$

where $f(z) = 0, 1, 1 - z, z, X$ is the longitudinal momentum fraction and Y^- represents the spatial coordinates. One can prove that the second derivative of the above expression vanishes at $k_T = 0$,

$$\nabla_{k_T}^2 \frac{\ell_{\mathbf{T}} \cdot (\ell_{\mathbf{T}} - f(z)\mathbf{k}_{\mathbf{T}})}{\ell_{\mathbf{T}}^2 (\ell_{\mathbf{T}} - f(z)\mathbf{k}_{\mathbf{T}})^2} = 0. \quad (93)$$

Therefore, all contributions from the asymmetrical-cut(right-cut and left-cut) diagrams will vanish after we take the second partial derivative with respect to k_T when we keep only the leading terms up to $\mathcal{O}(x_B/Q^2\ell_T^2)$,

$$\nabla_{k_T}^2 \overline{H}_{asym}^D|_{k_T=0} = 0 + \mathcal{O}(x_B/Q^2\ell_T^2). \quad (94)$$

In the same way we find that some of the central-cut diagrams will not contribute to the final results, either. In fact, after taking the second partial derivative with respect to k_T only four central-cut diagrams shown in Fig. 25 will contribute to the final result.

Including only those contributions that do not vanish after the second derivative with respect to k_T , we have

$$\begin{aligned} \nabla_{k_T}^2 \overline{H}^D|_{k_T=0} = & \int d\ell_T^2 \frac{\alpha_s}{2\pi} \frac{1+z^2}{1-z} e^{i(x+x_L)p^+y^-} \frac{2\pi\alpha_s}{N_c} \theta(-y_2^-) \theta(y^- - y_1^-) \\ & \times \left[\frac{4C_A}{\ell_T^4} (1 - e^{-ix_L p^+ y_2^-}) (1 - e^{-ix_L p^+ (y^- - y_1^-)}) \right. \\ & + \frac{4C_F(1-z)^2}{\ell_T^4} e^{-ix_L p^+ (y^- - y_1^-)} e^{-ix_L p^+ y_2^-} \\ & + \frac{2C_A(1-z)}{\ell_T^4} e^{-ix_L p^+ y_2^-} (1 - e^{-ix_L p^+ (y^- - y_1^-)}) \\ & + \left. \frac{2C_A(1-z)}{\ell_T^4} e^{-ix_L p^+ (y^- - y_1^-)} (1 - e^{-ix_L p^+ y_2^-}) \right] \\ & + \mathcal{O}(x_B/Q^2\ell_T^2) . \end{aligned} \quad (95)$$

The first term at the right-hand side in Eq.(95) comes from the contribution of $\overline{H}_{C(a)}^D$ which is the main contribution in the helicity amplitude approximation^{69,70}. It contains hard-soft, double hard processes and their interferences. The other three terms come from diagram (b),(c),(d) of Fig. 25 respectively. They constitute corrections to the first term in powers of $1-z$. The second term that is proportional to $(1-z)^2$ is from the final state radiation from the quark in the double hard process in Fig. 25(b). The third and fourth terms are the results of the interference of the final state radiation from the quark and other radiation processes (initial state radiation and radiation from the gluon line). They contain both double hard processes and interferences between hard-soft and double hard processes in Fig. 25(c) and (d).

Substituting Eq.(95) into Eqs.(84) and (80), we have the semi-inclusive tensor from double quark-gluon scattering including the contribution be-

yond the helicity amplitude approximation,

$$\begin{aligned} \frac{W_{\mu\nu}^{D,q}}{dz_h} &= \sum_q \int dx H_{\mu\nu}^{(0)}(xp, q) \int_{z_h}^1 \frac{dz}{z} D_{q \rightarrow h}(z_h/z) \frac{\alpha_s}{2\pi} C_A \frac{1+z^2}{1-z} \\ &\times \int \frac{d\ell_T^2}{\ell_T^4} \frac{2\pi\alpha_s}{N_c} \left[T_{qq}^A(x, x_L) + (1-z)T_{qq}^{A(1)}(x, x_L) \right. \\ &\quad \left. + \frac{C_F}{C_A}(1-z)^2 T_{qq}^{A(2)}(x, x_L) \right], \end{aligned} \quad (96)$$

where

$$\begin{aligned} T_{qq}^A(x, x_L) &= \int \frac{dy^-}{2\pi} dy_1^- dy_2^- (1 - e^{-ix_L p^+ y_2^-})(1 - e^{-ix_L p^+(y^- - y_1^-)}) \\ &\times e^{i(x+x_L)p^+ y^-} \theta(-y_2^-) \theta(y^- - y_1^-) \\ &\times \frac{1}{2} \langle A | \bar{\psi}_q(0) \gamma^+ F_{\sigma^+}(y_2^-) F^{+\sigma}(y_1^-) \psi_q(y^-) | A \rangle, \end{aligned} \quad (97)$$

$$\begin{aligned} T_{qq}^{A(1)}(x, x_L) &= \int \frac{dy^-}{2\pi} dy_1^- dy_2^- e^{i(x+x_L)p^+ y^-} \left[e^{-ix_L p^+(y^- - y_1^-)} + e^{-ix_L p^+ y_2^-} \right. \\ &\quad \left. - 2e^{-ix_L p^+(y^- - y_1^- + y_2^-)} \right] \theta(-y_2^-) \theta(y^- - y_1^-) \\ &\times \frac{1}{4} \langle A | \bar{\psi}_q(0) \gamma^+ F_{\sigma^+}(y_2^-) F^{+\sigma}(y_1^-) \psi_q(y^-) | A \rangle, \end{aligned} \quad (98)$$

$$\begin{aligned} T_{qq}^{A(2)}(x, x_L) &= \int \frac{dy^-}{2\pi} dy_1^- dy_2^- e^{ix p^+ y^- + ix_L p^+(y_1^- - y_2^-)} \theta(-y_2^-) \theta(y^- - y_1^-) \\ &\times \frac{1}{2} \langle A | \bar{\psi}_q(0) \gamma^+ F_{\sigma^+}(y_2^-) F^{+\sigma}(y_1^-) \psi_q(y^-) | A \rangle \end{aligned} \quad (99)$$

are twist-four parton matrix elements of the nucleus. Evidently these parton matrix elements are not independent of each other. $T_{qq}^A(x, x_L)$ has the complete four terms of soft-hard, double hard processes and their interferences. Therefore it contains essentially four independent parton matrix elements. $T_{qq}^{A(1)}(x, x_L)$ and $T_{qq}^{A(2)}(x, x_L)$ are the results of the corrections beyond the helicity amplitude approximation. But these two matrix elements are already contained in $T_{qq}^A(x, x_L)$.

During the collinear expansion, we have kept ℓ_T finite and took the limit $k_T \rightarrow 0$. As a consequence, the gluon field in one of the twist-four parton matrix elements in Eqs.(97)-(99) carries zero momentum in the soft-hard process. However, the gluon distribution $x f_g(x)$ at $x = 0$ is not defined in QCD. As argued in Refs.^{69,70}, this is due to the omission of higher order terms in the collinear expansion. As a remedy to the problem, a subset of the higher-twist terms in the collinear expansion can be resummed to

restore the phase factors such as $\exp(ix_T p^+ y^-)$, where $x_T \equiv \langle k_T^2 \rangle / 2p^+ q^- z$ is related to the intrinsic transverse momentum of the initial partons. As a result, soft gluon fields in the parton matrix elements will carry a fractional momentum x_T .

Using the factorization approximation^{69,70,102,101}, we can relate the twist-four parton matrix elements of the nucleus to the twist-two parton distributions of nucleons and the nucleus,

$$T_{qq}^A(x, x_L) = \frac{C}{x_A} (1 - e^{-x_L^2/x_A^2}) [f_q^A(x + x_L) x_T f_g^N(x_T) + f_q^A(x)(x_L + x_T) f_g^N(x_L + x_T)], \quad (100)$$

where C is a constant, $x_A = 1/MR_A$, $f_q^A(x)$ is the quark distribution inside a nucleus, and $f_g^N(x)$ is the gluon distribution inside a nucleon. A Gaussian distribution in the light-cone coordinates was assumed for the nuclear distribution, $\rho(y^-) = \rho_0 \exp(y^{-2}/2R_A^{-2})$, where $R_A^- = \sqrt{2}R_A M/p^+$ and M is the nucleon mass. We should emphasize that the twist-four matrix element is proportional to $1/x_A = R_A M$, or the nuclear size¹⁰¹.

Notice that the off-diagonal matrix elements that correspond to the interferences between hard-soft and double hard processes are suppressed by a factor of $\exp(-x_L^2/x_A^2)$. This is because in the interferences between double-hard and hard-soft processes, there is actually momentum flow of $x_L p^+$ between the two nucleons that the initial quark and gluon come from. Without strong long range two-nucleon correlation inside a nucleus, the amount of momentum flow $x_L p^+$ should then be restricted to the amount allowed by the uncertainty principle, $1/R_A^- \sim p^+/R_A M$. Similarly, the other two-parton matrix elements in Eqs.(98) and (99) can be approximated as

$$T_{qq}^{A(1)}(x, x_L) = \frac{C}{2x_A} \{ [f_q^A(x + x_L) x_T f_g^N(x_T) + f_q^A(x)(x_L + x_T) f_g^N(x_L + x_T)] e^{-x_L^2/x_A^2} - 2f_q^A(x)(x_L + x_T) f_g^N(x_L + x_T) \}, \quad (101)$$

$$T_{qq}^{A(2)}(x, x_L) = \frac{C}{x_A} f_q^A(x)(x_L + x_T) f_g^N(x_L + x_T). \quad (102)$$

From the above estimate of the matrix elements, both $T_{qq}^A(x, x_L)$ and $T_{qq}^{A(1)}(x, x_L)$ contain a factor $1 - e^{-x_L^2/x_A^2}$ because of the LPM interference effect. Such an interference factor will effectively cut off the integration over the transverse momentum at $x_L \sim x_A$ in Eq.(96). As we will show later in the calculation of the effective energy loss, the integration with such a restriction in the transverse momentum due to LPM interference effect will

give rise to a factor $1/x_A$ in addition to the coefficient $f_q^A(x)/x_A$. Consequently, contributions from double scattering in Eq.(96) that are associated with $T_{qq}^A(x, x_L)$ and $T_{qq}^{A(1)}(x, x_L)$ will be proportional to $R_A^2 f_q^A(x)$. These are the leading double scattering contributions in the limit of a large nuclear size. On the other hand, the third term $T_{qq}^{A(2)}(x, x_L)$ in Eq.(96), which does not contain any interference effect, will only contribute to a correction that is proportional to $R_A f_q^A(x)$. In the limit of a large nucleus, $A^{1/3} \gg 1$, we will neglect this term in our study of the double scattering processes.

4.3. Virtual Corrections

So far we have not considered virtual corrections which will ensure the final result to be infrared safe. The calculation of the virtual corrections can be calculated similarly as the radiative corrections. On the other hand, they can also be obtained via unitarity requirement. When cast into the DGLAP evolution equation as Eq.(73), the real corrections can be interpreted as the probability for the quark to radiate a gluon with momentum fraction $1 - z$. Then one must also take into account the probability of no gluon radiation in the evolution to ensure unitarity. Such unitarity requirement gives rise to the same virtual correction as calculated from the virtual diagrams. The virtual contribution to the quark fragmentation in double scattering processes is, for example,

$$\begin{aligned} \frac{W_{\mu\nu}^{D(v),q}}{dz_h} &= - \sum_q \int dx H_{\mu\nu}^{(0)}(xp, q) D_{q \rightarrow h}(z_h) \\ &\times \frac{\alpha_s}{2\pi} C_A \int_0^1 dz \frac{1+z^2}{1-z} \int \frac{d\ell_T^2}{\ell_T^4} \frac{2\pi\alpha_s}{N_c} T_{qq}^{A(m)}(x, x_L), \end{aligned} \quad (103)$$

where

$$T_{qq}^{A(m)}(x, x_L) \equiv T_{qq}^A(x, x_L) + (1-z)T_{qq}^{A(1)}(x, x_L). \quad (104)$$

Assuming a function $F(z)$ which is sufficiently smooth at $z = 1$, One can single out the infrared divergent part of the following integral,

$$\begin{aligned} \int_0^1 dz \frac{1+z^2}{1-z} F(z) &= F(1) \int_0^1 dz \frac{2}{1-z} - \Delta F; \\ \Delta F &\equiv \int_0^1 dz \frac{1}{1-z} [2F(1) - (1+z^2)F(z)]. \end{aligned} \quad (105)$$

The second term ΔF is finite since $F(z)$ is a smooth function of z .

We can apply this procedure to the integral in the modified fragmentation function. The divergent term can be combined with the radiative contribution in Eq.(96) to cancel the infrared divergency. With the help of the ‘+’function¹⁰⁰, the final result can be expressed as

$$\begin{aligned} \frac{W_{\mu\nu}^{D,q}}{dz_h} &= \sum_q \int dx H_{\mu\nu}^{(0)}(xp, q) \frac{2\pi\alpha_s}{N_c} \int \frac{d\ell_T^2}{\ell_T^4} \int_{z_h}^1 \frac{dz}{z} D_{q \rightarrow h}(z_h/z) \frac{\alpha_s}{2\pi} C_A \\ &\times \left[\frac{1+z^2}{(1-z)_+} T_{qg}^{A(m)}(x, x_L) + \delta(z-1) \Delta T_{qg}^{A(m)}(x, \ell_T^2) \right]; \quad (106) \end{aligned}$$

$$\begin{aligned} \Delta T_{qg}^{A(m)}(x, \ell_T^2) &\equiv \int_0^1 dz \frac{1}{1-z} \left[2T_{qg}^{A(m)}(x, x_L)|_{z=1} \right. \\ &\quad \left. - (1+z^2)T_{qg}^{A(m)}(x, x_L) \right]. \quad (107) \end{aligned}$$

Here the implicit z -dependence of $T_{qg}^{A(m)}(x, x_L)$ plays an important role in the final result. The above integrand will be proportional to the splitting function for a single scattering if one ignores the z dependence of $T_{qg}^A(x, x_L)$. Similarly, the final result for contributions from gluon fragmentation is

$$\begin{aligned} \frac{W_{\mu\nu}^{D,g}}{dz_h} &= \sum_q \int dx H_{\mu\nu}^{(0)}(xp, q) \frac{2\pi\alpha_s}{N_c} \int \frac{d\ell_T^2}{\ell_T^4} \int_{z_h}^1 \frac{dz}{z} D_{g \rightarrow h}(z_h/z) \\ &\times \frac{\alpha_s}{2\pi} C_A \left[\frac{1+(1-z)^2}{z_+} T_{qg}^{A(m)}(x, x_L) + \delta(z) \Delta T_{qg}^{A(m)}(x, \ell_T^2) \right], \quad (108) \end{aligned}$$

where we have used the fact that x_L in Eq.(87) is invariant under the transform $z \rightarrow 1-z$ and so is $T_{qg}^A(x, x_L)$.

4.4. Modified Fragmentation Function and Parton Energy Loss

Including these virtual corrections and the single scattering contribution, we can rewrite the semi-inclusive tensor in terms of a modified fragmentation function $\tilde{D}_{q \rightarrow h}(z_h, \mu^2)$,

$$\frac{dW_{\mu\nu}}{dz_h} = \sum_q \int dx \tilde{f}_q^A(x, \mu_I^2) H_{\mu\nu}^{(0)}(x, p, q) \tilde{D}_{q \rightarrow h}(z_h, \mu^2) \quad (109)$$

where $\tilde{f}_q^A(x, \mu_I^2)$ is the quark distribution function which in principle should also include the higher-twist contribution¹⁰⁵ of the initial state scattering.

The modified effective quark fragmentation function is defined as

$$\begin{aligned} \tilde{D}_{q \rightarrow h}(z_h, \mu^2) &\equiv D_{q \rightarrow h}(z_h, \mu^2) \\ &+ \int_0^{\mu^2} \frac{d\ell_T^2}{\ell_T^2} \frac{\alpha_s}{2\pi} \int_{z_h}^1 \frac{dz}{z} [\Delta\gamma_{q \rightarrow qg}(z, x, x_L, \ell_T^2) D_{q \rightarrow h}(z_h/z) \\ &+ \Delta\gamma_{q \rightarrow gq}(z, x, x_L, \ell_T^2) D_{g \rightarrow h}(z_h/z)] , \end{aligned} \quad (110)$$

where $D_{q \rightarrow h}(z_h, \mu^2)$ and $D_{g \rightarrow h}(z_h, \mu^2)$ are the leading-twist fragmentation functions. The modified splitting functions are given as

$$\begin{aligned} \Delta\gamma_{q \rightarrow qg}(z, x, x_L, \ell_T^2) &= \left[\frac{1+z^2}{(1-z)_+} T_{qg}^{A(m)}(x, x_L) + \delta(1-z) \Delta T_{qg}^{A(m)}(x, \ell_T^2) \right] \\ &\times \frac{2\pi\alpha_s C_A}{\ell_T^2 N_c \tilde{f}_q^A(x, \mu_T^2)} , \end{aligned} \quad (111)$$

$$\Delta\gamma_{q \rightarrow gq}(z, x, x_L, \ell_T^2) = \Delta\gamma_{q \rightarrow qg}(1-z, x, x_L, \ell_T^2). \quad (112)$$

To further simplify the calculation, we assume $x_T \ll x_L \ll x$. The modified parton matrix elements can be approximated by

$$T_{qg}^{A(m)}(x, x_L) \approx \frac{\tilde{C}}{x_A} (1 - e^{-x_L^2/x_A^2}) f_q^A(x) \left[1 - \frac{1-z}{2} \right] , \quad (113)$$

where $\tilde{C} \equiv 2C x_T f_g^N(x_T)$ is a coefficient which should in principle depend on Q^2 and x_T . Here we will simply take it as a constant.

In the above matrix element, one can identify $1/x_L p^+ = 2q^- z(1-z)/\mu^2$ as the formation time of the emitted gluons. For large formation time as compared to the nuclear size, the above matrix element vanishes, demonstrating a typical LPM interference effect. This is because the emitted gluon (with long formation time) and the leading quark are still a coherent system when they propagate through the nucleus. Additional scattering will not induce more gluon radiation, thus limiting the energy loss of the leading quark.

The reduction of phase space available for gluon radiation due to the LPM interference effect is critical for applying the LQS formalism to the problem in this paper. In the original LQS approach¹⁰², the generalized factorization for processes with a large final transverse momentum $\ell_T^2 \sim Q^2$ allows one to consider the leading contribution in $1/Q^2$, which is enhanced by the nuclear size $R_A \sim A^{1/3}$. For large Q^2 and A , the higher-twist contribution from double parton rescattering that is proportional to $\alpha_s R_A/Q^2$ will then be the leading nuclear correction. One can neglect contributions

from more than two parton rescattering. In deriving the modified fragmentation functions, we however have to take the leading logarithmic approximation in the limit $\ell_T^2 \ll Q^2$, where ℓ_T is the transverse momentum of the radiated gluon. Since the LPM interference suppresses gluon radiation whose formation time ($\tau_f \sim Q^2/\ell_T^2 p^+$) is larger than the nuclear size MR_A/p^+ in our chosen frame, ℓ_T^2 should then have a minimum value of $\ell_T^2 \sim Q^2/MR_A \sim Q^2/A^{1/3}$. Here M is the nucleon mass. Therefore, the logarithmic approximation is still valid for large nuclei ($MR_A \gg 1$). In the meantime, the leading higher-twist contribution proportional to $\alpha_s R_A/\ell_T^2 \sim \alpha_s R_A^2/Q^2$ can still be small for large Q^2 so that one can neglect processes with more than two parton rescattering. The parameter for twist expansion of the fragmentation processes inside a nucleus is thus $\alpha_s A^{2/3}/Q^2$ as compared to $\alpha_s A^{1/3}/Q^2$ for processes with large final transverse momentum as studied by LQS¹⁰². This is why the nuclear modification to the fragmentation function as derived in this paper depends quadratically on the nuclear size R_A .

Because of momentum conservation, the fractional momentum in a nucleon is limited to $x_L < 1$. Though the Fermi motion effect in a nucleus can allow $x_L > 1$, the parton distribution in this region is still significantly suppressed. It therefore provides a natural cut-off for x_L in the integration over z and ℓ_T in Eq.(110). With the assumption of the factorized form of the twist-4 nuclear parton matrices, there is only one free parameter $\tilde{C}(Q^2)$ which represents quark-gluon correlation strength inside nuclei. Once it is fixed, one can predict the z , energy and nuclear dependence of the medium modification of the fragmentation function. Shown in Figs. 26 and 27 are the calculated nuclear modification factor of the fragmentation functions for ^{14}N and ^{84}Kr targets as compared to the recent HERMES data¹⁰⁶. There are strong correlations among values of Q^2 , ν and z in the HERMES data which are also taken in account in our calculation. The predicted shape of the z - and ν -dependence agrees well with the experimental data. A remarkable feature of the prediction is the quadratic $A^{2/3}$ nuclear size dependence, which is verified for the first time by an experiment. This quadratic dependence comes from the combination of the QCD radiation spectrum and the modification of the available phase space in ℓ_T or x_L due to the LPM interferences. Note that the numerical results shown here are obtained with the original helicity amplitude approximation^{69,70}. The numerical calculation beyond the helicity approximation differs only about a few percent¹⁰⁴.

By fitting the overall suppression for one nuclear target, we obtain the only parameter in our calculation, $\tilde{C}(Q^2) = 0.0060 \text{ GeV}^2$ with

JET QUENCHING AND RADIATIVE ENERGY LOSS IN DENSE NUCLEAR MATTER 57

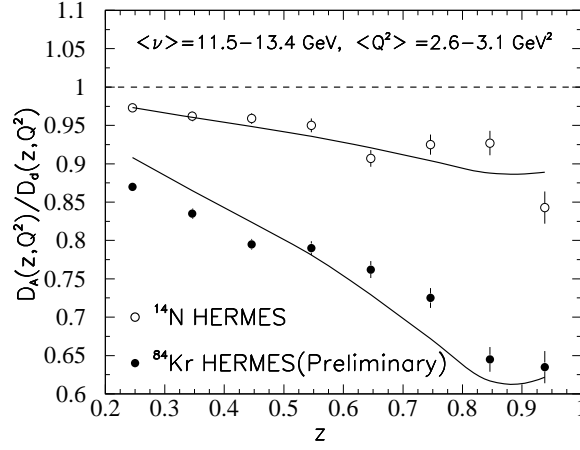


Fig. 26. Predicted nuclear modification of jet fragmentation function is compared to the HERMES data¹⁰⁶ on ratios of hadron distributions between A and d targets in DIS.

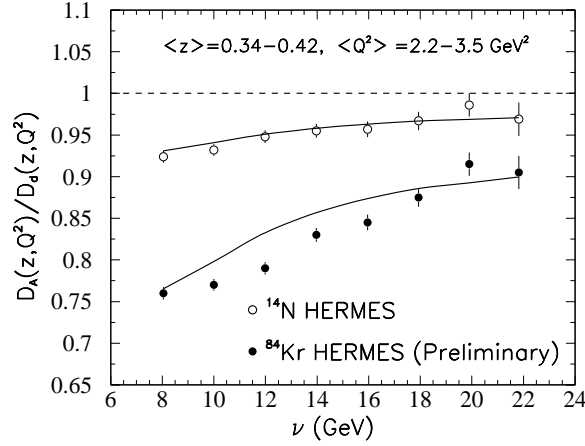


Fig. 27. Energy dependence of the nuclear modification compared with the HERMES data¹⁰⁶.

$\alpha_s(Q^2) = 0.33$ at $Q^2 \approx 3 \text{ GeV}^2$. This parameter is also related to nuclear broadening of the transverse momentum of the Drell-Yan dilepton in pA collisions¹⁰⁷, $\langle \Delta q_{\perp}^2 \rangle \approx \tilde{C} \pi \alpha_s / N_c x_A$. With an experimental¹⁰⁸ value of $\langle \Delta q_{\perp}^2 \rangle = 0.016 A^{1/3} \text{ GeV}^2$ and $\alpha_s(M_{ll}^2) = 0.21$ ($\langle M_{ll}^2 \rangle \approx 40 \text{ GeV}^2$), one finds $\tilde{C}(M_{ll}^2) = 0.013 \text{ GeV}^2$, which is about a factor 2 larger than the

value obtained in our fit to the HERMES data. The value of \tilde{C} determined from nuclear broadening in photo-production of a di-jet is even larger¹⁰² at $Q^2 = 4p_T^2 \approx 64 \text{ GeV}^2$. Such a strong scale dependence of $\tilde{C}(Q^2)$ is in line with one's expectation, since it is related to gluon distribution $xg(x, Q^2)$ at small x in nuclei¹⁰¹.

In principle the modification of the fragmentation functions would be the only experimental effect of induced gluon radiation via multiple scattering. One can never directly measure the energy loss of the leading quark. The net effect of the energy loss is the suppression of leading particles on one hand and the enhancement of soft particles on the other, leading to the modification of the fragmentation functions. One can then experimentally characterize the parton energy loss via the momentum transfer from large to small momentum regions of the fragmentation functions.

Upon a close examination of Eq.(110), we see that the first term is the renormalized fragmentation function in vacuum. The rest is particle production induced by the rescattering of the quark through the nuclear medium. In particular, the last term is particle production from the fragmentation of the gluon which is induced by the secondary scattering. Such particle production is at the expense of the energy loss of the leading quark. We can thus quantify the quark energy loss by the momentum fraction carried by the radiated gluon,

$$\begin{aligned} \langle \Delta z_g \rangle(x_B, \mu^2) &= \int_0^{\mu^2} \frac{d\ell_T^2}{\ell_T^2} \int_0^1 dz \frac{\alpha_s}{2\pi} z \Delta\gamma_{q \rightarrow gq}(z, x_B, x_L, \ell_T^2) \\ &= \frac{C_A \alpha_s^2}{N_c} \int_0^{\mu^2} \frac{d\ell_T^2}{\ell_T^4} \int_0^1 dz [1 + (1-z)^2] \frac{T_{qg}^{A(m)}(x_B, x_L)}{f_q^A(x_B, \mu_T^2)}. \end{aligned} \quad (114)$$

Using the approximation for the modified twist-four parton matrix elements in Eq.(113), we have

$$\begin{aligned} \langle \Delta z_g \rangle(x_B, \mu^2) &= \tilde{C} \frac{C_A \alpha_s^2}{N_c} \frac{x_B}{x_A Q^2} \int_0^1 dz \frac{1 + (1-z)^2}{z(1-z)} \\ &\quad \times \int_0^{x_\mu} \frac{dx_L}{x_L^2} \left(1 - \frac{z}{2}\right) (1 - e^{-x_L^2/x_A^2}), \end{aligned} \quad (115)$$

where $x_\mu = \mu^2/2p^+q^-z(1-z) = x_B/z(1-z)$ if we choose the factorization scale as $\mu^2 = Q^2$. When $x_A \ll x_B \ll 1$ we can estimate the leading quark

energy loss roughly as

$$\langle \Delta z_g \rangle(x_B, \mu^2) \approx \tilde{C} \frac{C_A \alpha_s^2}{N_c} \frac{x_B}{Q^2 x_A^2} 5\sqrt{\pi} \left[\ln \frac{1-2x_B}{x_B} - \frac{1}{2} \right]. \quad (116)$$

Since $x_A = 1/MR_A$, the energy loss $\langle \Delta z_g \rangle$ thus depends quadratically on the nuclear size.

In the rest frame of the nucleus, $p^+ = m_N$, $q^- = \nu$, and $x_B \equiv Q^2/2p^+q^- = Q^2/2m_N\nu$. One can get the averaged total energy loss as $\Delta E = \nu \langle \Delta z_g \rangle \approx \tilde{C}(Q^2)\alpha_s^2(Q^2)m_N R_A^2 (C_A/N_c) 3 \ln(1/2x_B)$. With the determined value of \tilde{C} , $\langle x_B \rangle \approx 0.124$ in the HERMES experiment¹⁰⁶ and the average distance $\langle L_A \rangle = R_A \sqrt{2/\pi}$ for the assumed Gaussian nuclear distribution, one gets the quark energy loss $dE/dL \approx 0.5$ GeV/fm inside a Au nucleus.

4.5. Energy Loss in Hot Medium at RHIC

To extend our study of modified fragmentation functions to jets in heavy-ion collisions and to relate to results obtained in the opacity expansion approach, we can assume $\langle k_T^2 \rangle \approx \mu^2$ (the Debye screening mass) and a gluon density profile $\rho(y) = (\tau_0/\tau)\theta(R_A - y)\rho_0$ for a 1-dimensional expanding system. Since the initial jet production rate is independent of the final gluon density which can be related to the parton-gluon scattering cross section⁵⁷ [$\alpha_s x_T G(x_T) \sim \mu^2 \sigma_g$], one has then

$$\frac{\alpha_s T_{qg}^A(x_B, x_L)}{f_q^A(x_B)} \sim \mu^2 \int dy \sigma_g \rho(y) [1 - \cos(y/\tau_f)], \quad (117)$$

where $\tau_f = 2Ez(1-z)/\ell_T^2$ is the gluon formation time. One can recover the form of energy loss in a thin plasma obtained in the opacity expansion approach³⁶,

$$\begin{aligned} \langle \Delta z_g \rangle &= \frac{C_A \alpha_s}{\pi} \int_0^1 dz \int_0^{\frac{Q^2}{\mu^2}} du \frac{1 + (1-z)^2}{u(1+u)} \\ &\times \int_{\tau_0}^{R_A} d\tau \sigma_g \rho(\tau) \left[1 - \cos \left(\frac{(\tau - \tau_0) u \mu^2}{2Ez(1-z)} \right) \right]. \end{aligned} \quad (118)$$

Keeping only the dominant contribution and assuming $\sigma_g \approx C_a 2\pi \alpha_s^2 / \mu^2$ ($C_a=1$ for qg and $9/4$ for gg scattering), one obtains the averaged energy loss,

$$\left\langle \frac{dE}{dL} \right\rangle \approx \frac{\pi C_a C_A \alpha_s^3}{R_A} \int_{\tau_0}^{R_A} d\tau \rho(\tau) (\tau - \tau_0) \ln \frac{2E}{\tau \mu^2}. \quad (119)$$

Neglecting the logarithmic dependence on τ , the averaged energy loss in a 1-dimensional expanding system can be expressed as

$$\langle \frac{dE}{dL} \rangle_{1d} \approx \frac{dE_0}{dL} \frac{2\tau_0}{R_A}, \quad (120)$$

where $dE_0/dL \propto \rho_0 R_A$ is the energy loss in a static medium with the same gluon density ρ_0 as in a 1-d expanding system at time τ_0 . Because of the expansion, the averaged energy loss $\langle dE/dL \rangle_{1d}$ is suppressed as compared to the static case and does not depend linearly on the system size. This could be one of the reasons why the effect of parton energy loss is found to be negligible in AA collisions at $\sqrt{s} = 17.3$ GeV¹⁰⁹.

An effective model of modified fragmentation functions was proposed in Ref.^{44,45}:

$$\tilde{D}_{a \rightarrow h}(z) \approx \frac{1}{1 - \Delta z} D_{a \rightarrow h} \left(\frac{z}{1 - \Delta z} \right), \quad (121)$$

with Δz to account for the fractional parton energy loss. This effective model is found to reproduce the pQCD result from Eq.(110) very well, but only when Δz is set to be $\Delta z \approx 0.6 \langle z_g \rangle$. Therefore the actual averaged parton energy loss should be $\Delta E/E = 1.6 \Delta z$ with Δz extracted from the effective model. The factor 1.6 is mainly caused by the unitarity correction effect in the pQCD calculation. A similar effect is also found in the opacity expansion approach⁴⁷.

Both PHENIX and STAR experiments have reported^{1,5} strong suppression of high p_T hadrons in central $Au + Au$ collisions at $\sqrt{s} = 130$ and 200 GeV, indicating for the first time a large parton energy loss in heavy-ion collisions. To extract the parton energy loss, we compare the data with the calculated hadron p_T spectra in heavy-ion collisions using the above effective model for medium modified jet fragmentation functions³⁹. Shown in Fig. 28 are the nuclear modification factors $R_{AA}(p_T)$ as the ratios of hadron spectra in AA (pA) and pp collisions normalized by the number of binary collisions²⁵. Parton shadowing and nuclear broadening of the intrinsic k_T are also taken into account in the calculation which describes pA data for energies up to $\sqrt{s} = 40$ GeV³⁹. The nuclear k_T -broadening gives the Cronin enhancement at large p_T in pA collisions, where there is no parton energy loss induced by a hot medium. Fitting the PHENIX data yields $\langle dE/dL \rangle_{1d} \approx 0.34(\ln E / \ln 5)$ GeV/fm, including the factor of 1.6 from the unitarity correction effect. We consider only π^0 data here, since at large p_T the charged hadrons are dominated by baryons, which could be influenced mainly by non-perturbative dynamics³⁶.

JET QUENCHING AND RADIATIVE ENERGY LOSS IN DENSE NUCLEAR MATTER 61

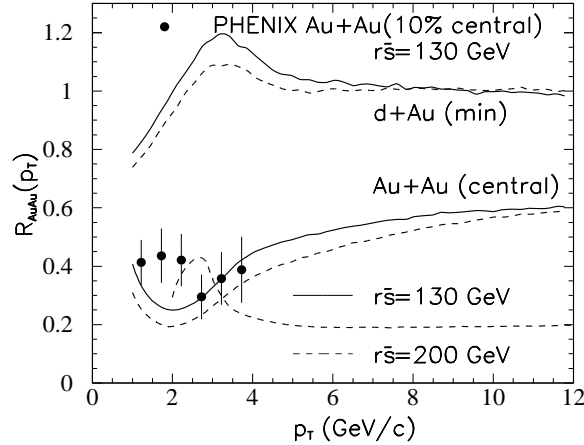


Fig. 28. Calculated nuclear modification factor of π^0 p_T spectra for $d + Au$ and central $Au + Au$ collisions at $\sqrt{s} = 130$ (solid) and 200 GeV (dashed) as compared to PHENIX data¹. The lower dashed line uses the energy loss as given in Eq.(122).

Taking into account the expansion, the averaged parton energy loss extracted from the PHENIX data would be equivalent to $(dE/dL)_0 = 0.34(R_A/2\tau_0) \ln E / \ln 5$ in a static system with the same gluon density as the initial value of the expanding system at τ_0 . With $R_A \sim 6$ fm and $\tau_0 \sim 0.2$ fm, this would give $(dE/dL)_0 \approx 7.3$ GeV/fm for a 10-GeV parton, which is about 15 times of that in a cold Au nucleus, as extracted from the HERMES data. Since the parton energy loss is directly proportional to gluon density of the medium, this implies that the gluon density in the initial stage of $Au + Au$ collisions at $\tau_0 = 0.2$ fm/c is about 15 times higher than that inside a cold nucleus. We can predict the π^0 spectra at $\sqrt{s} = 200$ GeV as given by the dashed lines in Fig. 28, assuming that the initial parton density in central $Au + Au$ collisions at $\sqrt{s} = 200$ GeV is about 10% higher than at 130 GeV.

In Fig. 28, we have shown the predicted suppression factor at large p_T with the same logarithmic energy-dependence of the energy loss as in the cold nuclear matter which gives a suppression factor that increases with p_T . However, new RHIC data³ at 200 GeV show a constant suppression factor at larger p_T . This might be the indication of the importance of the detailed balance⁹⁸ which gives much stronger energy dependence of the energy loss. We show as the lower dashed line in Fig. 28 the result for an effective parton

energy loss

$$\Delta E \propto (E/\mu - 1.6)^{1.20}/(7.5 + E/\mu) \quad (122)$$

which is parameterized according to the result from Ref.⁹⁸ where both stimulated gluon emission and thermal absorption are included in the calculation of the total energy loss. The detailed balance between emission and absorption both reduces the effective parton energy loss and increases the energy dependence. The threshold is the consequence of gluon absorption that competes with radiation that effectively shuts off the energy loss. The parameter μ is set to be 1 GeV in the calculation shown in Fig. 28.

5. Summary

In this report we reviewed two recent approaches to the problem of non-Abelian radiative energy energy loss in dense but finite QCD matter. In the first section, we highlighted some of the striking new high p_T phenomena observed for the first time in $A + A$ reactions at RHIC with $\sqrt{s} > 100$ AGeV. An interesting pattern of hadron suppression, already beginning at moderate $p_T > 3$ GeV, was seen in the hadron flavor dependence of single inclusive spectra, in the large azimuthal asymmetry, and in the preliminary two-hadron correlations. We interpret these phenomena as manifestations of jet quenching in ultra-dense matter produced in such reactions. Our predictions for these phenomena in both approaches are reviewed in later sections and depend on the energy loss, $\Delta E = \int dx dE/dx$, of fast quarks and gluons propagating through rapidly expanding QCD matter. The two approaches, GLV and WW/WOGZ reviewed here, provide a systematic way to compute ΔE via an opacity or higher twist expansion in finite nuclear matter. Elsewhere reviewed asymptotic approaches such as the BDMS/Z/SW^{68,110} are designed for applications to “thick” or macroscopic media at asymptotic energies. An analytic approximation to the sum of the infinite multiple collision series is obtained through an approximate color dipole quantum diffusion analogous to the Moliere series in electrodynamics. The complications due to finite kinematic bounds are neglected. As shown in¹¹¹, the phenomenological applications of the asymptotic expressions tend to overpredict quenching at RHIC and lead to a too rapid variation of the suppression factor with p_T , inconsistent with the RHIC data. In our approach, on the other hand, the opacity series is computed to arbitrary order in opacity for applications to finite opacity systems where the non-Gaussian (Rutherford) tails of distributions are not yet eclipsed by

*JET QUENCHING AND RADIATIVE ENERGY LOSS IN DENSE NUCLEAR MATTER*63

the approximate Gaussian small p_T component. In addition, our expressions can be applied to arbitrary 3D expanding and time dependent media such as created in nuclear collisions.

The GLV reaction operation approach discussed in Section 2 is based on a general algebraic recursive method that describes the propagation and interaction of systems through dense nuclear matter, taking into account the severe destructive LPM interference effects due to the long formation times of ultra-relativistic partons. It provides a means to compute the multiple collision amplitudes to any order χ^n in the opacity $\chi = \int dz \sigma \rho$. So far it has been successfully applied to obtain solutions for the nuclear broadening⁷⁴ and the final state medium induced radiation^{52,53} resulting from multiple elastic and inelastic projectile scatterings. The range of applicability of the calculations can be significantly extended by careful treatment of kinematic bounds.

The final state double differential distributions of jets and gluons are presented as an infinite series in powers of the mean number of scatterings χ . For elastic scatterings this series can be summed to all orders (or equivalently all twist parton-parton correlations) to reproduce the standard Glauber theory result, but more general than the simple color dipole approximation used in asymptotic analyses. For inelastic processes, a closed sum to all orders can unfortunately only be carried out in the dipole approximation as in BDMS/Z/SW (see¹¹⁰ for most recent developments). However, our analytic^{52,74} expressions at any finite order in opacity can be evaluated numerically^{52,53}. Numerical evaluation of the expressions through the first three orders (up to twist 8) has been carried out for phenomenological applications. Each power in opacity adds a twist 2 parton-parton correlation. Future work via this approach includes computation of multiple gluon emission beyond the Poisson approximation and the broadening and radiation of dipole-like, possibly heavy, $\bar{q}q$ systems. Applications to heavy quark energy loss including both the Ter-Mikayelian gluon dispersion effects as well as the “dead cone” effect are also underway¹¹².

The WW approach reviewed in Section 3 extends the calculation of energy loss to include the positive feedback (jet acceleration) due to absorption of thermal gluons in the medium. Absorption counteracts the induced energy loss for jet momenta less than the typical thermal energy scale $\sim 3T$. In an expanding hydrodynamic medium with transverse boost rapidity η_T we expect that this absorption feedback contribution is blue shifted to higher momenta $p_T \sim 3Te^{\eta_T}$. Thus jet quenching cannot suppress the spectrum below the local equilibrium hydrodynamic limit.

In Section 4, several recent works were combined (referred to as the WOGZ approach^{69,70,101,104}) to elaborate on a general twist-expansion of multiple parton scattering beyond the GW model of the medium. In that approach one can calculate explicitly the modified parton fragmentation function up to twist 4 thus far. The LPM interference effect is then embedded in the twist-four parton matrix elements of the nucleus which also contains the fundamental properties of the nuclear medium – parton density correlations inside a nucleus. These matrix elements replace the Debye screened interactions used in the GLV approach. One can demonstrate explicitly that the quadratic dependence of the modification of fragmentation functions and the effective parton energy loss on the nuclear size R_A is caused both by the LPM interference and the specific form of gluon radiation spectra in QCD. The predicted nuclear modification of the fragmentation function, both the energy and nuclear dependence, is found to agree well with the recent experimental data¹⁰⁶ on jet fragmentation in $e + A$. This is an important test of both the twist or opacity expansions since it shows the dominance of the twist 4 (first order in opacity) contribution to the energy loss in finite nuclear systems as found numerically in the GLV expansion up to twist 8. Extending the results to a parton propagating in a hot QCD medium, we have shown that the twist expansion to order 4 is equivalent to the first order opacity GLV result under certain simplifying assumptions about the form of the twist 4 matrix elements. The phenomenological application of WOGZ to both DIS on cold nuclear targets and high-energy heavy-ion collisions suggests that the parton energy loss in an expanding system at RHIC would be equivalent to $(dE/dx)_0 \approx 7.3$ GeV/fm in a static medium, which is almost 15 times higher than that in a cold Au nucleus.

If the jet quenching pattern is confirmed by further measurements and theoretical refinements, current RHIC data may have already provided the first tomographic evidence that initial parton densities on the order of 100 times nuclear matter density were achieved in $Au + Au$ collisions. The full analysis of the flavor composition, shape, and azimuthal moments of the high p_T spectra appears to be a promising diagnostic probe of the evolution of the produced quark-gluon plasma.

However, in spite of the consistency of our jet tomography analysis with current RHIC data, it is still too early to draw definitive conclusions. The main uncertainty is the magnitude of gluon shadowing¹¹³ in the initial nuclear wavefunction. While estimates of shadowing vary wildly, unfortunately nothing is yet known experimentally on this important question.

*JET QUENCHING AND RADIATIVE ENERGY LOSS IN DENSE NUCLEAR MATTER*⁶⁵

QCD analysis¹¹⁴ suggests that non-linear corrections to DGLAP evolution may cause the gluon density to saturate at small x . Saturation is found in classical Yang-Mills models^{115,116,117,118} as well. In Ref.¹¹⁹ it was proposed that gluon saturation or shadowing phenomena alone may account for a significant part of the observed high p_T hadron suppression pattern. Our estimates of shadowing based on ESK'98⁴⁸ do not support this idea and neither do recent calculations^{120,121} in the MQ approach¹¹⁴ of the upper limit of the saturation scale and the rate of disappearance of its effects on the small and moderate p_T spectra. Fortunately, a decisive experimental test is now under way at RHIC via $d + Au$ reactions. If our theory is correct, and the observed suppression pattern in $Au + Au$ is due to jet quenching via final state interactions in the dense QCD matter produced, then instead of suppression, the Cronin effect is predicted to dominate over shadowing in the $x > 0.01$ range accessible at RHIC. We therefore predict as an upper limit an *enhancement* of the moderate p_T hadrons by $\sim 10 - 30\%$ in $d + A$ relative to binary scaled $p + p$. On the other hand, if the saturation model is correct, and the suppression pattern in $Au + Au$ is a consequence of deep gluon shadowing in the initial state, then a suppression about 30% of moderate and high p_T hadrons is predicted to occur in $d + Au$ ¹¹⁹.

The experimental answer to this decisive question may be known by the publication time of this review. In either case, the answer will be exciting.

Acknowledgments

M.G. and I.V. gratefully acknowledge extensive collaboration with Peter Levai on the GLV approach. X.N.W. and B.W.Z. would like to thank Enke Wang on extensive collaboration on the WW approach with detailed balance and many fruitful discussions. X.N.W. would also like to acknowledge collaborations with X. F. Guo and J. Osborne on the twist expansion approach. This work was supported by the Director, Office of Energy Research, Office of High Energy and Nuclear Physics, Division of Nuclear Physics, and by the Office of Basic Energy Science, Division of Nuclear Science, of the U.S. Department of Energy under Contracts No. DE-FG02-87ER40371, DE-FG02-93ER40764, and DE-AC03-76SF00098 and by National Natural Science Foundation of China under project No. 19928511 and No. 10135030.

References

1. K. Adcox *et al.* [PHENIX Collaboration], arXiv:nucl-ex/0207009.

2. C. Adler *et al.*, Phys. Rev. Lett. **89**, 202301 (2002).
3. S. Mioduszewski [PHENIX Collaboration], arXiv:nucl-ex/0210021.
4. D. d'Enterria [PHENIX Collaboration], arXiv:hep-ex/0209051.
5. G. J. Kunde [STAR Collaboration], arXiv:nucl-ex/0211018.
6. C. Adler *et al.* [STAR Collaboration], arXiv:nucl-ex/0210033.
7. C. Adler *et al.* [STAR Collaboration], Phys. Rev. Lett. **90**, 032301 (2003).
8. K. Filimonov [STAR Collaboration], arXiv:nucl-ex/0210027.
9. P. Levai, G. Papp, G. Fai, M. Gyulassy, G. G. Barnafoldi, I. Vitev and Y. Zhang, Nucl. Phys. A **698**, 631 (2002).
10. Proc. 15th Int. Ultra. Nucleus-Nucleus Coll. (Quark Matter 2001, Jan. SUNY), Nucl.Phys. A **698** (2002) 1c; Proc. 16th (Quark Matter 2002, July Nantes, France); Nucl. Phys. A in press.
11. J. D. Bjorken, FERMILAB-PUB-82-59-THY and erratum (unpublished)
12. M. H. Thoma and M. Gyulassy, Nucl. Phys. B **351**, 491 (1991).
13. M. H. Thoma, Phys. Rev. D **49**, 451 (1994).
14. D. A. Appel, Phys. Rev. D **33**, 717 (1986).
15. J. P. Blaizot and L. D. McLerran, Phys. Rev. D **34**, 2739 (1986).
16. M. Rammerstorfer and U. W. Heinz, Phys. Rev. D **41**, 306 (1990).
17. M. Gyulassy and M. Plumer, Phys. Lett. B **243**, 432 (1990).
18. M. Gyulassy and M. Plumer, Nucl. Phys. A **527**, 641 (1991).
19. M. Gyulassy, M. Plumer, M. Thoma and X. N. Wang, Nucl. Phys. A **538**, 37C (1992).
20. X. N. Wang and M. Gyulassy, Phys. Rev. D **44**, 3501 (1991).
21. X. N. Wang and M. Gyulassy, Phys. Rev. D **45**, 844 (1992).
22. M. Gyulassy and X. N. Wang, Comput. Phys. Commun. **83**, 307 (1994).
23. X. N. Wang and M. Gyulassy, Phys. Rev. Lett. **68**, 1480 (1992).
24. M. M. Aggarwal *et al.* [WA98 Collaboration], Phys. Rev. Lett. **81**, 4087 (1998) [Erratum-ibid. **84**, 578 (1998)].
25. X. Wang and M. Gyulassy, Phys. Rev. Lett. **86**, 3496 (2001).
26. E. Wang and X. N. Wang, Phys. Rev. C **64**, 034901 (2001)
27. C. Adler *et al.* [STAR Collaboration], Nucl. Phys. A **698**, 64 (2002).
28. W. A. Zajc *et al.* [PHENIX Collaboration], Nucl. Phys. A **698**, 39 (2002).
29. G. Roland [PHOBOS Collaboration], Nucl. Phys. A **698** 54 (2002).
30. I. G. Bearden *et al.* [BRAHMS Collaboration], Nucl. Phys. A **698**, 29 (2002).
31. P. F. Kolb, P. Huovinen, U. W. Heinz and H. Heiselberg, Phys. Lett. B **500**, 232 (2001).
32. P. Huovinen, P. F. Kolb, U. W. Heinz, P. V. Ruuskanen and S. A. Voloshin, Phys. Lett. B **503**, 58 (2001).
33. P. F. Kolb, U. W. Heinz, P. Huovinen, K. J. Eskola and K. Tuominen, Nucl. Phys. A **696**, 197 (2001).
34. D. Teaney, J. Lauret and E. V. Shuryak, nucl-th/0104041.
35. X. N. Wang, Phys. Rev. C **63**, 054902 (2001).
36. M. Gyulassy, I. Vitev and X. N. Wang, Phys. Rev. Lett. **86**, 2537 (2001).
37. M. Pluemer, M. Gyulassy and X. N. Wang, Nucl. Phys. A **590**, 511C (1995).
38. J. F. Owens, Rev. Mod. Phys. **59** (1987) 465.
39. X. N. Wang, Phys. Rev. C **61**, 064910 (2000).

JET QUENCHING AND RADIATIVE ENERGY LOSS IN DENSE NUCLEAR MATTER 67

40. I. Vitev, arXiv:nucl-th/0302002.
41. K. J. Eskola and H. Honkanen, Nucl. Phys. A **713**, 167 (2003).
42. I. Vitev, arXiv:hep-ph/0212109.
43. X. N. Wang, Phys. Rev. C **58**, 2321 (1998).
44. X. N. Wang, Z. Huang and I. Sarcevic, Phys. Rev. Lett. **77**, 231 (1996).
45. X. N. Wang and Z. Huang, Phys. Rev. C **55**, 3047 (1997).
46. R. Baier, Y. L. Dokshitzer, A. H. Mueller and D. Schiff, JHEP **0109**, 033 (2001).
47. M. Gyulassy, P. Levai and I. Vitev, Phys. Lett. B **538**, 282 (2002).
48. K. J. Eskola, V. J. Kolhinen and C. A. Salgado, Eur. Phys. J. C **9**, 61 (1999).
49. L. D. Landau and I. Pomeranchuk, Dokl. Akad. Nauk Ser. Fiz. **92**, 535 (1953).
50. L. D. Landau and I. Pomeranchuk, Dokl. Akad. Nauk Ser. Fiz. **92**, 735 (1953).
51. A. B. Migdal, Phys. Rev. **103**, 1811 (1956).
52. M. Gyulassy, P. Levai and I. Vitev, Nucl. Phys. B **594**, 371 (2001).
53. M. Gyulassy, P. Levai and I. Vitev, Phys. Rev. Lett. **85**, 5535 (2000).
54. M. Gyulassy, P. Levai and I. Vitev, Nucl. Phys. B **571**, 197 (2000).
55. M. Gyulassy, P. Levai and I. Vitev, Nucl. Phys. A **661**, 637 (1999).
56. R. Baier, Y. L. Dokshitzer, A. H. Mueller, S. Peigne and D. Schiff, Nucl. Phys. B **483**, 291 (1997).
57. R. Baier, Y. L. Dokshitzer, A. H. Mueller, S. Peigne and D. Schiff, Nucl. Phys. B **484**, 265 (1997).
58. R. Baier, Y. L. Dokshitzer, A. H. Mueller and D. Schiff, Nucl. Phys. B **531**, 403 (1998).
59. R. Baier, Y. L. Dokshitzer, A. H. Mueller and D. Schiff, Phys. Rev. C **60**, 064902 (1999).
60. B. G. Zakharov, JETP Lett. **63**, 952 (1996).
61. B. G. Zakharov, JETP Lett. **65**, 615 (1997).
62. B. G. Zakharov, JETP Lett. **73**, 49 (2001).
63. B. G. Zakharov, JETP Lett. **76**, 201 (2002).
64. U. A. Wiedemann, Nucl. Phys. A **690**, 731 (2001).
65. U. A. Wiedemann, Nucl. Phys. B **588**, 303 (2000).
66. U. A. Wiedemann, Nucl. Phys. B **582**, 409 (2000).
67. C. A. Salgado and U. A. Wiedemann, Phys. Rev. Lett. **89**, 092303 (2002).
68. R. Baier, D. Schiff and B. G. Zakharov, Ann. Rev. Nucl. Part. Sci. **50**, 37 (2000).
69. X. N. Wang and X. F. Guo, Nucl. Phys. A **696**, 788 (2001).
70. X. F. Guo and X. N. Wang, Phys. Rev. Lett. **85**, 3591 (2000).
71. E. Wang and X. N. Wang, Phys. Rev. Lett. **89**, 162301 (2002).
72. M. Gyulassy and X. Wang, Nucl. Phys. B **420**, 583 (1994). ; Wang X N, Gyulassy M, Plumer M, Phys. Rev. D **51** (1995) 3436.
73. M. Gyulassy, I. Vitev, X. N. Wang and P. Huovinen, Phys. Lett. B **526**, 301 (2002).
74. M. Gyulassy, P. Levai and I. Vitev, Phys. Rev. D **66**, 014005 (2002). I. Vitev and J.W. Qiu, work in preparation.

75. I. Vitev and M. Gyulassy, Phys. Rev. Lett. **89**, 252301 (2002).
76. A. Accardi, arXiv:hep-ph/0212148.
77. Y. Zhang, G. Fai, G. Papp, G. G. Barnafoldi and P. Levai, Phys. Rev. C **65**, 034903 (2002).
78. B. Z. Kopeliovich, J. Nemchik, A. Schafer and A. V. Tarasov, Phys. Rev. Lett. **88**, 232303 (2002).
79. F. Arleo, Phys. Lett. B **532**, 231 (2002).
80. J. Velkovska [PHENIX collaboration], Nucl. Phys. A **698**, 507 (2002).
81. K. Adcox *et al.* [PHENIX Collaboration], Phys. Rev. Lett. **88**, 242301 (2002).
82. N. Xu and M. Kaneta, Nucl. Phys. A **698**, 306 (2002).
83. C. Adler *et al.* [STAR Collaboration], Phys. Rev. Lett. **87**, 262302 (2001).
84. K. Adcox *et al.* [PHENIX Collaboration], Phys. Rev. Lett. **89**, 092302 (2002).
85. C. Adler *et al.* [STAR Collaboration], Phys. Rev. Lett. **89**, 092301 (2002) [arXiv:nucl-ex/0203016].
86. I. Vitev and M. Gyulassy, Phys. Rev. C **65**, 041902 (2002).
87. I. Vitev and M. Gyulassy, arXiv:hep-ph/0208108.
88. I. Vitev, M. Gyulassy and P. Levai, arXiv:hep-ph/0109198.
89. G. C. Rossi and G. Veneziano, Nucl. Phys. B **123**, 507 (1977).
90. L. Montanet, G. C. Rossi and G. Veneziano, Phys. Rept. **63**, 149 (1980).
91. D. Kharzeev, Phys. Lett. B **378**, 238 (1996).
92. S. E. Vance and M. Gyulassy, Phys. Rev. Lett. **83**, 1735 (1999).
93. S. E. Vance, M. Gyulassy and X. N. Wang, Phys. Lett. B **443**, 45 (1998).
94. J. Y. Ollitrault, Phys. Rev. D **46**, 229 (1992).
95. E. V. Shuryak, Phys. Rev. C **66**, 027902 (2002).
96. T. Hirano and Y. Nara, arXiv:nucl-th/0301042.
97. T. Hirano and Y. Nara, arXiv:nucl-th/0211096.
98. E. Wang and X. N. Wang, Phys. Rev. Lett. **87**, 142301 (2001).
99. E. Braaten and R. D. Pisarski, Nucl. Phys. B **337**, 569 (1990).
100. V. N. Gribov and L. N. Lipatov, Sov. J. Nucl. Phys. **15**, 438 (1972); Yu. L. Dokshitzer, Sov. Phys. JETP **46**, 641 (1977); G. Altarelli and G. Parisi, Nucl. Phys. **B126**, 298 (1977);
101. J. Osborne and X.-N. Wang, Nucl. Phys. A **710**, 281 (2002) [arXiv:hep-ph/0204046].
102. M. Luo, J. Qiu and G. Sterman, Phys. Lett. **B279**, 377 (1992); M. Luo, J. Qiu and G. Sterman, Phys. Rev. D **50**, 1951 (1994); M. Luo, J. Qiu and G. Sterman, Phys. Rev. D **49**, 4493 (1994).
103. J. Qiu, Phys. Rev. D **42**, 30 (1990).
104. B. W. Zhang and X.-N. Wang, arXiv:hep-ph/0301195.
105. A. H. Mueller and J. Qiu, Nucl. Phys. **B268**, 427 (1986).
106. A. Airapetian *et al.* [HERMES Collaboration], Eur. Phys. J. C **20**, 479 (2001); V. Muccifora [HERMES Collaboration], arXiv:hep-ex/0106088.
107. X. F. Guo, Phys. Rev. D **58**, 114033 (1998).
108. P. L. McGaughy, J. M. Moss and J. C. Peng, Ann. Rev. Nucl. Part. Sci. **49**, 217 (1999); J. C. Peng, private communication.

*JET QUENCHING AND RADIATIVE ENERGY LOSS IN DENSE NUCLEAR MATTER*69

109. X.-N. Wang, Phys. Rev. Lett. **81**, 2655 (1998).
110. Note Added in Proof: On completion of this report an instructive new analysis comparing the BDMS/Z/SW and the GLV approaches became available: C. A. Salgado and U. A. Wiedemann, arXiv:hep-ph/0302184; U. A. Wiedemann, arXiv:hep-ph/0302194.
111. F. Arleo, JHEP **0211**, 044 (2002).
112. M. Djordjevic and M. Gyulassy, arXiv:nucl-th/0302069.
113. N. Armesto and C. A. Salgado, arXiv:hep-ph/0301200.
114. A. H. Mueller and J. w. Qiu, Nucl. Phys. B **268**, 427 (1986).
115. L. D. McLerran and R. Venugopalan, Phys. Rev. D **50**, 2225 (1994).
116. L. D. McLerran and R. Venugopalan, Phys. Rev. D **49**, 3352 (1994).
117. E. Iancu, A. Leonidov and L. McLerran, arXiv:hep-ph/0202270.
118. A. H. Mueller, arXiv:hep-ph/0111244.
119. D. Kharzeev, E. Levin and L. McLerran, arXiv:hep-ph/0210332.
120. K. J. Eskola, H. Honkanen, V. J. Kolhinen, J. W. Qiu and C. A. Salgado, arXiv:hep-ph/0211239.
121. K. J. Eskola, H. Honkanen, V. J. Kolhinen, J.W. Qiu and C. A. Salgado, arXiv:hep-ph/0302185.